Submitted to ADVANCED FUNCTIONAL MATERIALS

DOI: 10.1002/adfm.((please insert DOI)

Silaindacenodithiophene based low band gap polymers – the effect of fluorine substitution on device performances and film morphologies.

By *Bob C. Schroeder, Zhenggang Huang, Raja Shahid Ashraf,* Jeremy Smith, Pasquale D' Angelo, Scott E. Watkins, Thomas D. Anthopoulos, James R. Durrant* and *Iain McCulloch*

B. C. Schroeder, Z. Huang, Dr. R. S. Ashraf, Prof. J. R. Durrant, Prof. I. McCulloch
Department of Chemistry and Centre for Plastic Electronics
Imperial College London
London, SW7 2AZ (United Kingdom)
E-mail: r.ashraf@imperial.ac.uk

Dr. J. Smith, Dr. P. D'Angelo, Dr. T. D. Anthopoulos
Department of Physics and Centre for Plastic Electronics
Imperial College London
London, SW7 2AZ (United Kingdom)

Dr. S. E. Watkins
CSIRO Materials Science and Engineering
Melbourne, VIC 3169 (Australia)

Keywords: silaindacenodithiophene, hole mobility, solar cell, fluorine, conjugated polymers

Abstract: Silaindacenodithiophene is co-polymerized with benzo[*c*][1,2,5]thiadiazole (**BT**) and 4,7-di(thiophen-2-yl)benzo[*c*][1,2,5]thiadiazole (**DTBT**), respectively their fluorinated counter parts 5,6-difluorobenzo[*c*][1,2,5]thiadiazole (**2FBT**) and 5,6-difluoro-4,7-di(thiophen-2-yl) benzo[*c*][1,2,5]thiadiazole (**2FDTBT**). The influence of the thienyl spacers and fluorine atoms on molecular packing and active layer morphology is investigated with regard to device performances. BHJ solar cells based on silaindacenodithiophene donor-acceptor polymers achieved PCE's of 4.5% and hole mobilities of as high as 0.28 $cm^2/(Vs)$ were achieved in OFET.

1. Introduction

Over the last decade organic semi-conducting polymers have received a lot of attention, with their performances in organic field effect transistors (OFET) and organic photovoltaic devices

(OPV) increasing significantly.[1] The improved performance is not only the result of a better understanding of the physics governing the various charge generating and transport processes and the improved processing techniques, but also due to the development of new donor-acceptor semiconducting materials.[2]

Silole based building blocks, such as dithienosilole and indacenodithiophene (**IDT**), have proven their potential in OPVs, as well as in OFETs, when introduced into donor-acceptor polymers.[3] Extended π-conjugated ladder type monomers like indacenodithiophene are attractive for incorporation into donor-acceptor polymers partly because the backbone rigidification leads to an improved conjugation length (enhanced coplanarity of repeat units), resulting in higher short-circuit currents (J_{SC}) due to an improved long wavelength photon absorption. Besides the improved optical properties, the silicon bridge stiffens the polymer backbone and reduces conformational disorder. This reduction in energetic disorder has been reported to increase the charge carrier mobility.[4] Recently the introduction of silicon atoms into the indacenodithiophene backbone was observed to provide high photocurrent efficiencies and high charge carrier mobilities.[5] In addition, the separation between the anti-bonding lobes located on the carbon atoms of linked aryl rings in the indacenodithiophene unit increases, and this reduction in antibonding energy manifests as a reduction in the HOMO energy level, thus leading to an increase in the open-circuit voltage (V_{OC}) of solar cells. It is also possible in some cases to have effective orbital mixing between the silicon's σ^*-orbital and the π^*-orbital of the adjacent butadiene fragment, stabilizing the LUMO, with correspondingly lower bandgaps than their carbon bridged counterparts.[6]

Recently, several groups have reported fluorine substituted conjugated polymers with high-efficiency solar cells.[7] Fluorine is smaller in size than other electron withdrawing groups (*e.g.* cyano or trifluoromethyl groups) and can be introduced within the polymer backbone without causing too much steric hindrance.

The co-polymerization of silaindacenodithiophene (**SiIDT**) with benzo[*c*][1,2,5]thiadiazole (**BT**), 4,7-di(thiophen-2-yl)benzo[*c*][1,2,5]thiadiazole (**DTBT**) respectively, has led to high V_{OC} values in OPV devices.[5] We expect to further increase the OPV performances of **SiIDT** based polymers by increasing the V_{OC} of the aforementioned polymers due to the introduction of electron-withdrawing fluorine atoms on the polymer backbone, thus lowering the polymer's HOMO energy level and potentially increasing the PCE.[7a, 8] Herein we report the co-polymerization of 5,6-difluorobenzo[*c*][1,2,5]thiadiazole (**2FBT**) and 5,6-difluoro-4,7-di(thiophen-2-yl) benzo[*c*][1,2,5]thiadiazole (**2FDTBT**) with the **SiIDT** donor moiety. The influence of the thienyl spacers and the fluorine atoms on molecular packing and active layer morphology will be evaluated with regard to device performance.

2. Results and Discussion

2.1. Synthesis

The silaindacenodithiophene (**SiIDT**) monomer was obtained according to our previously published synthetic pathway.[5b] All four copolymers shown in **Scheme 1** were synthesized by Stille cross-coupling reactions under microwave heating conditions, yet two different catalytic systems and solvents respectively, were used depending on the aryl groups to couple. In the case where the stannylated **SiIDT** monomer was coupled to a phenyl ring, tetrakis(triphenylphosphine) palladium was used as catalyst and *o*-xylene as solvent. However, when the **SiIDT** unit was coupled to a thienyl group, tris(dibenzylideneacetone) dipalladium, together with tri(*o*-tolyl) phosphine was used as catalytic system in chlorobenzene.

It is essential for the performance of OFETs and OPVs to employ high quality semi-conducting materials, *i.e.* the polymer should have no structural defects and contain neither organic, nor inorganic impurities. By using metal catalyzed coupling reactions, the probability of structural defects in the polymer chain can be minimized, but there is typically no

deliberate control over the chemical nature of the chain ends, unless an endcapping step at the end of the polymerization is used. Even though the concentration of end-groups is very low in a polymer chain of typical molecular weight, their effects on charge trapping, hysteresis and film morphology can be significant.[9] In order to avoid these undesirable effects, all the synthesized polymers were end-capped with chemically inert phenyl groups. Organic and inorganic impurities were removed by precipitating the polymer in methanol, followed by Soxhlet extractions with polar and non-polar solvents. After the Soxhlet extractions, the polymer was dissolved in chloroform and washed with an aqueous sodium diethyldithiocarbamate solution to remove residual palladium impurities.

All polymers were synthesized with high molecular weights and comparable polymerization degrees, with the **SiIDT-BT** polymer having the highest molecular weight (M_n=30.0 kg/mol). The molecular weights of all polymers are summarized in **Table 1**. The polymers are readily soluble in common organic solvents, except for the fluorinated polymers, which will only dissolve when heated in chlorinated solvents. Thermal gravimetric analysis (TGA) confirmed the stability of all the polymers and a 5% weight loss could not be observed at temperatures lower than 400°C (see Figure S18 in the Supporting Information). Differential scanning calorimetry (DSC) shows a broad melt around 310°C with a sharper crystallisation on cooling at around 290°C for **SiIDT-BT**, but for all the other polymers no obvious thermal transitions were identified in the temperature range of 0 to 350°C (see Figure S19 to S23 in the Supporting Information).

2.2. Optical Properties

The UV-*vis.* absorption spectra of the polymers in dilute chlorobenzene solution and thin-films spin-coated on glass substrates are shown in **Figure 1**. The detailed absorption data,

including absorption maxima in solution and film, as well as the corresponding absorption onsets and bandgaps are presented in **Table 2**.

Even though the polymer backbones of **SiIDT-BT** and **SiIDT-2FBT** are very similar and the fluorine atoms are small in size, they have a large influence on the molecular packing. In solution, the absorption feature of **SiIDT-2FBT** is blue-shifted by 40 nm compared to **SiIDT-BT**. The blue-shift is partially attributed to its lower molecular weight and the presence of fluorine on the benzothiadiazole (**BT**) unit. The atomic radius of fluorine (0.50 Å) is larger than that of hydrogen (0.25 Å) and expected to give rise to steric hindrance between the fluorine atoms on the **BT** unit and the adjacent thiophene of the **SiIDT** moiety.[10] We attribute the blue shift of the absorption spectrum to the reduced conjugation length of **SiIDT-2FBT**. In the solid state however, the backbone twist is suppressed due to planarising intramolecular interactions between the fluorine atoms on the **BT** core and the sulfur atom on the neighboring **SiIDT** unit, resulting in similar absorption peaks for **SiIDT-BT** and **SiIDT-2FBT** with a more pronounced vibronic structure compared to the solution absorption spectra.[11] In the case of **SiIDT-DTBT** and **SiIDT-2FDTBT** the influence of the fluorine atoms on the backbone twist is diminished because the additional thiophene ring between the **SiIDT** moiety and the **BT** core acts as a spacer, thus minimizing the sterical hindrance between the two bulkier aromatic units.

Both polymers, **SiIDT-BT** and **SiIDT-2FBT**, exhibit two well defined absorption peaks, one at higher energies resulting from π-π* transitions and a more important one at lower energies caused by the internal charge transfer (ICT) from the donor to the acceptor part of the polymer backbone. A different behavior can be observed, when thienyl spacers are introduced between the donor and acceptor parts of the polymer backbone, as it is the case for **SiIDT-DTBT** and **SiIDT-2FDTBT**. The UV-*vis.* spectra still present two different absorption features, but they are less defined as in the previous case. For both polymers, the π-π*

transition peaks are more intense and observed at longer wavelengths, compared to the absorption peaks of **SiIDT-BT** and **SiIDT-2FBT**, resembling rather low-wavelength shoulders than independent peaks.

The ionization potentials of all polymers were measured by ultraviolet photoelectron spectroscopy in air (UV-PESA) and cyclic voltammetry (CV); the results are summarized in **Table 2**. The measured energy levels follow the same trends within both techniques, but there are significant differences when comparing the data from both techniques. These differences emphasize that it is very difficult to measure the frontier-orbital energy levels accurately because the values obtained depend not only on the experimental technique, but can also be influenced by the morphology, hence, and the measured energy levels should be regarded as estimated values. PESA, as well as CV measurements, confirm that the introduction of electron withdrawing fluorine atoms lower both HOMO and LUMO energy levels to a similar degree, and thus have a negligible effect on the bandgap of **SiIDT-2FBT** and **SiIDT-2FDTBT** compared to their non-fluorinated counter-parts.

Quantum mechanical calculations were performed to predict the energy levels and model the molecular orbital distributions. Density functional theory calculation, using B3LYP/6-31G* model, were performed on trimers with methyl substituted alkyl chains for simplicity. In our study, the theoretical values were all higher in energy than the experimental values, which we attribute to limitations within the DFT model to describe low-band gap semi-conducting polymers.[12] Nevertheless, the calculated values are consistent with the trends observed in the experimental PESA and CV data. The calculations predict lower lying HOMO energy levels for the fluorinated polymers, as well as increase in the HOMO when thienyl spacers are introduced between the donor and acceptor parts of the polymer backbone. The theoretical calculations predict furthermore a delocalization of the HOMO over the entire polymer backbone and a preferential localization of the LUMO on the **BT** moiety for all four **BT**

containing polymers. The molecular orbitals of **SiIDT-2FBT** and **SiIDT-2FDTBT** are depicted in **Figure 2**; the energy distributions for **SiIDT-BT** and **SiIDT-DTBT** can be found in the supporting information.

2.3. Field-Effect Transistor Devices

Field effect transistors with top-gate, bottom-contact device architecture were fabricated to investigate the charge carrier mobility of **SiIDT** based polymers. After thermal annealing at 180°C, the hole mobilities were extracted from the transfer characteristics in saturation and are summarized in **Table 3**. The fluorine-sulfur interactions were expected to favor polymer backbone planarization, potentially therefore reducing intermolecular packing distances and thus having a positive effect on hole mobility. However the opposite effect is observed experimentally, both fluorinated polymers (**SiIDT-2FBT** and **SiIDT-2FDTBT)** exhibit lower hole mobilities, 0.004 cm^2/Vs and 0.19 cm^2/Vs, than their non-fluorinated counterparts. It is speculated that the lower electron density on the polymer backbone, induced by the presence of fluorine atoms, hinders hole mobility, or hole injection, which compensates the beneficial effect of backbone planarity. The introduction of thienyl spacers into the polymer backbone however, has a positive effect on the hole mobility (0.28 cm^2/Vs and 0.19 cm^2/Vs). **SiIDT-DTBT** and **SiIDT-2FDTBT** exhibit several orders of magnitude higher hole mobilities, than the polymers with no spacers in the backbone. The transfer curves and output characteristics of the OFET devices can be found in the Supporting Information. To understand this significant difference in mobility, drop cast polymer films were annealed for 10 minutes at 180°C and probed by X-ray diffraction (XRD). The complete XRD spectra of all four **SiIDT** polymers before and after annealing can be found in the Supporting Information. As can be seen in the diffraction patterns presented in **Figure 3**, **SiIDT-BT** and **SiIDT-2FBT** both show intense diffraction peaks at 5.3° and 10.6°, thus giving evidence for a crystalline

microstructure with a lamellar packing distance of 16.6 Å. Interestingly, the **SiIDT-BT** has a very amorphous microstructure before annealing, and only becomes highly ordered upon annealing at 180°C for 10 minutes.

We further investigated OFET devices based on **SiIDT-BT** before and after annealing, but the hole mobility remained virtually unchanged (0.012 cm^2/Vs before and 0.014 cm^2/Vs after annealing). However a considerable shift in threshold voltage from -7 V before to -27 V after annealing was observed. The polymer film morphology was investigated by AFM before and after annealing (See **Figure S26** in the Supporting Information) and a surface roughening was noticed. We attribute the threshold voltage increase in part to the possible introduction of new trap states at the dielectric interface formed during the crystallization of the polymer at high annealing temperatures, and corresponding surface roughening.

On the other hand, **SiIDT-DTBT** and **SiIDT-2FDTBT** were found to be less crystalline than the aforementioned polymers, showing broader and less intense diffraction peaks at 5.1°, respectively 5.3°. The diffraction peak of **SiIDT-DTBT** is sharper (FWHM = 0.46) than the one for **SiIDT-2FDTBT** (FWHM = 1.23), thus indicating a higher degree of crystallinity. In addition, a change in the position of the diffraction peak of **SiIDT-DTBT** (5.1°) compared to **SiIDT-2FDTBT** (5.3°) is observed, which translates into a larger lamellar stacking distance of 17.4 Å. It is worth mentioning, that in this study the least crystalline polymers, **SiIDT-DTBT** and **SiIDT-2FDTBT**, gave the highest mobilities. In previously published reports it has also been found that polymers that do not exhibit a high degree of long range order can lead to high hole mobilities, believed to be due to excellent one dimensional transport along the polymer backbone with short favourable hops between chains facilitating charge percolation.[13]

3.4. Photovoltaic Properties

To evaluate the photovoltaic performances of the **SiIDT** polymers, bulk hetero-junction (BHJ) solar cells with conventional device structure consisting of ITO/PEDOT:PSS/Polymer:$PC_{71}BM$/Ca/Al were prepared and tested under simulated 100 mW cm^{-2} AM1.5G illumination. The J-V curves and external quantum efficiencies (EQE) of the organic photovoltaic cells (OPV) are presented in **Figure 4**. The corresponding open-circuit voltages (V_{OC}), short-circuit currents (J_{SC}), fill factors (FF) and power conversion efficiencies (PCE) are summarized in **Table 4**.

Figure 4 shows the external quantum efficiency (EQE) of the best devices of each blend ratio as a function of wavelength, which is consistent with the polymer/fullerene blends UV-*vis.* absorption spectra. Convolution of these EQE spectra with the AM1.5 spectra gave calculated short circuit current densities in good agreement (±0.5 mA cm^{-2}) with those measured under AM1.5 simulated sunlight (**Table 4**). The EQE spectrum of **SiIDT-DTBT** and **SiIDT-2FDTBT** extends further to the red than **SiIDT-BT**, consistent with the insertion of thienyl spacer leading to extended red absorption in these polymers. The EQE of both of these polymers extends up to 700 nm, while that of **SiIDT-BT** ranges only to 650 nm. We attribute the higher EQE response in the visible region to the corresponding strong absorbance of the blends, resulting from both the intrinsic absorption of the polymers and the presence of a high content of $PC_{71}BM$, which absorbs significantly at 400-500 nm. The broad coverage of the solar spectrum of the solar cell results in a desirable J_{SC} under illumination with white light. The device of **SiIDT-BT** blend exhibited a higher EQE response relative to other polymer blends with a maximum of 60% at about 518 nm, consistent to its higher photocurrent.

Devices based on **SiIDT-BT** and **SiIDT-DTBT** have been reported previously, with device efficiencies of up to 4.5%.[5] We expect to further increase the device performance by introducing fluorine atoms on the polymer backbone. However, the PCE of the device based on **SiIDT-2FBT** is heavily limited by its low $J_{SC,}$ despite the fact that the UV-*vis.* absorption

spectrum of **SiIDT-2FBT** is slightly more red-shifted than the **SiIDT-BT** one. The EQE spectra indicate that this loss of photocurrent results from a loss of photocurrent density from both polymer and $PC_{71}BM$ absorption. Photoluminescence (PL) quenching data indicated similar high polymer PL quenching for both polymers, indicating that this loss of photocurrent cannot be assigned to exciton diffusion limitations (see **Figure 5**). To evaluate further the lower J_{SC} for the **SiIDT-2FBT** /$PC_{71}BM$ device, the blend morphologies were investigated by close contact atomic force microscopy (AFM), as shown in **Figure 6**. While the topography image of **SiIDT-BT**/$PC_{71}BM$ shows a relative homogeneous film microstructure, large phase segregation (50-200 nm) is found in the topography image of **SiIDT-2FBT**/$PC_{71}BM$. Transmission electron microscopy (TEM) confirmed this difference in film microstructure, with excellent agreement between the AFM and TEM data (see **Figure 6**). The TEM data employed an iodine stain, with the more prevelant darker island evident in the TEM image corresponding to $PC_{71}BM$ rich domains. A similar phenomenon was observed by Yu and co-workers, who found that introducing fluorine to the polymer backbone changes initially homogenous blend morphology to a heterogeneous one with large phase segregation and non-bicontinuous features.[14] The extent to which the coarse film microstructure is the direct cause of the lower photocurrent for **SiIDT-2FBT**/$PC_{71}BM$ is not obvious. The PL quenching data indicates that the lower photocurrent is most probably not associated with exciton diffusion limitations, suggesting that the domains observed in the AFM and TEM images do not correspond to pure polymer and pure fullerene domains. Rather it appears more likely that this coarser domain structure reduces the efficiency of charge collection in the **SiIDT-2FBT**/$PC_{71}BM$ devices.

Although the HOMO energy levels for **SiIDT-BT** and **SiIDT-2FBT** measured by PESA and CV are very similar, a slightly larger V_{OC} is observed in the devices based on **SiIDT-2FBT** as expected from the DFT calculations. Devices based on **SiIDT-DTBT** display lower V_{OC} than

SiIDT-BT based devices due to the addition of the thienyl spacer, which primarily increases the π electron density, thus raising the HOMO energy level. The introduction of thienyl spacers into the polymer backbone also results in a finer blend microstructure (see **Figure 6**). **SiIDT-DTBT** based devices have similar J_{SC} and *FF* values as the **SiIDT-BT** polymer but the overall device performance is lower because of the smaller V_{OC}.

When devices employ **SiIDT-2FDTBT**, the addition of the thienyl spacers leads again to a smaller V_{OC} compared with **SiIDT-2FBT** based devices. However, there are significant improvements in both J_{SC} and *FF* which increase the device efficiency to 4.3%. The increase in photocurrent may be attributed to the red-shifted polymer absorption spectrum. Additionally, thienyl spacer introduction offers a much more homogeneous microstructure to **SiIDT-2FDTBT**/$PC_{71}BM$ compared with **SiIDT-2FBT**/$PC_{71}BM$ (see **Figure 6**).

4. Conclusion

In conclusion, we have synthesized a series of low-band gap polymers incorporating the **SiIDT** donor moiety and we investigated the effect of polymer fluorination on device performance and morphology. The incorporation of fluorine atoms to the polymer backbone was shown to influence both the polymer electronic energy levels and thin film morphology. The highest OPV device PCE achieved was 4.3% for the **SiIDT-2FDTBT polymer**, compared to 3.6% for its non-fluorinated counterpart. In field effect transistor devices, the **SiIDT** based polymers achieved high hole mobilities, up to 0.28 cm^2/Vs, with the unexpected trend being that the less crystalline thin films exhibited the higher mobilities.

5. Experimental Section

Characterization: Photo Electron Spectroscopy in Air (PESA) measurements were recorded with a Riken Keiki AC-2 PESA spectrometer with a power setting of 5nW and a power

number of 0.5. Number-average (M_n) and weight-average (M_w) molecular weights were determined with an Agilent Technologies 1200 series GPC in chlorobenzene at 80 °C, using two PL mixed B columns in series, and calibrated against narrow polydispersity polystyrene standards. Electron Ionization mass spectrometry were performed with a Micromass AutoSpec Premier mass spectrometer. UV-Vis absorption spectra were recorded on a UV-1601 Shimadzu UV-Vis spectrometer. AFM was performed on a 5500 AFM from Agilent Technology in tapping mode and TEM images were recorded on a high-resolution JEOL 2010 TEM (80-200 kV) with interchangeable pole-pieces. DSC experiments were carried out with a Metler Toledo DSC822 instrument. TGA plots were obtained with a Perkin Elmer Pyris 1 TGA. Cyclic voltammograms (CV) were obtained using a cylindrical platinum working electrode and a platinum mesh counter electrode in acetonitrile at a potential scan rate of 10 $mV \cdot s^{-1}$. Ag/Ag^+ was used as reference electrode and calibrated against ferrocene. All the measurements were carried out in an argon-saturated solution of 0.1 M of tetrabutylammonium hexafluorophosphate (*n*-Bu_4NPF_6) in anhydrous acetonitrile. X-ray diffraction (XRD) measurements were carried out with a PANALYTICAL X'PERT-PRO MRD diffractometer equipped with a nickel-filtered Cu $K\alpha_1$ beam and a X' CELERATOR detector, using a current of 40 mA and an accelerating voltage of 40 kV.

Polymer Synthesis: Condition A. A microwave vial was charged with bis(trimethylstannyl) monomer **1** (0.250 g, 0.233 mmol), 0.95 eq. of dibrominated monomer and 5 mol% of tetrakis(triphenylphosphine) palladium (0). The vial was sealed and 1 mL of *o*-xylene was added. The reaction mixture was degassed with argon during 30 minutes and submitted to the following temperature scheme in the microwave reactor: 5 minutes at 120°C, 5 minutes at 140°C, 5 minutes at 160°C and 40 minutes at 170°C. The reaction mixture was cooled down to room temperature and 0.1 eq. of bromobenzene was added in one portion by syringe. The mixture was resubmitted to the microwave reactor, 1 minute at 100°C, 1 minute at 120°C, 2

minutes at 140°C and 5 minutes at 160°C. Once the polymeric solution was cooled down, 0.1 eq. of trimethyl(phenyl)stannane was added by syringe. The reaction mixture was subjected on last time to the previously mentioned temperature scheme to finalize the end-capping reaction. After reaction, the crude polymer was precipitated in methanol and then further purified by Soxhlet extractions with acetone, hexane and chloroform, each for 24 hours. Remaining palladium residues were removed by treating a polymeric chloroform solution with an aqueous sodium diethyldithiocarbamate solution for 2 hours at 50°C under vigorous stirring. Afterwards the organic phase was separated from the aqueous phase and washed several times with water. The polymeric solution was concentrated under reduced pressure and precipitated into cold methanol. The recovered polymer was dried under high vacuum for at least 24 hours.

Condition B. A 5 mL microwave vial was charged with with bis(trimethylstannyl) monomer **1** (0.250 g, 0.233 mmol), 0.95 eq. of dibrominated monomer, 2 mol% of tris(dibenzylideneacetone)dipalladium (0) and 8 mol% of tri(*o*-tolyl) phosphine. The vial was sealed and chlorobenzene (1 mL) was added. The obtained solution was degassed with argon during 30 minutes. The vial was subjected to the following reaction conditions in the microwave reactor: 2 minutes at 100°C, 2 minutes at 120°C, 5 minutes at 140°C, 5 minutes at 160°C and 40 minutes at 170°C. The polymer was end-capped by addition of 0.1 eq. of bromobenzene before the reaction mixture was resubmitted to the microwave reactor, 1 minute at 100°C, 1 minute at 120°C, 2 minutes at 140°C and 5 minutes at 160°C. The polymeric solution was cooled down and 0.1 eq. of trimethyl(phenyl) stannane was added by syringe. The reaction vial was subjected to the previously mentioned temperature scheme to finalize the end-capping reaction. After reaction, the crude polymer was precipitated in methanol and then further purified by Soxhlet extractions with acetone, hexane and chloroform during 24 hours each. Remaining palladium residues were removed by treating a

polymeric chloroform solution with an aqueous sodium diethyldithiocarbamate solution for 2 hours at 50°C under vigorous stirring. Afterwards the organic phase was separated from the aqueous phase and washed several times with water. The polymeric solution was concentrated under reduced pressure and precipitated into cold methanol. The polymer was filtered off and dried under high vacuum for at least 24 hours.

SiIDT-BT. Dark-blue solid (135 mg, 0.131 mmol, 59%). M_n = 30.0 kg mol^{-1}, M_w = 58.9 kg mol^{-1}, PDI = 1.96. ^{1}H NMR (*o*-DCB-d$_4$, 400 MHz, 313 K, δ): 8.73 (s, 2H), 8.30 (s, 2H), 8.20-7.75 (bm, 2H), 1.91-1.71 (bm, 8H, SiCH$_2$), 1.63-1.50 (bm, 8H, CH$_2$), 1.49-1.18 (bm, 40H, CH$_2$), 1.04 (t, *J* = 7 Hz, 12H, CH$_3$).

SiIDT-DTBT. Dark-blue solid (151 mg, 0.13 mmol, 63%). M_n = 22.3 kg mol^{-1}, M_w = 56.6 kg mol^{-1}, PDI = 2.54. ^{1}H NMR (*o*-DCB-d$_4$, 400 MHz, 313 K, δ): 8.31 (s, 2H, Ar H), 8.19-8.07 (m, 2H, Ar H), 8.01-7.83 (bm, 2H, Ar H), 7.80-7.71 (m, 2H, Ar H), 7.67-7.45 (bm, 2H, Ar H), 1.85-1.69 (bm, 8H, CH$_2$), 1.61-1.52 (bm, 8H, CH$_2$), 1.50-1.23 (bm, 40H, CH$_2$), 1.07 (t, *J* = 7 Hz, 12H, CH$_3$).

SiIDT-2FBT. Dark-blue solid (102 mg, 0.11 mmol, 51%). M_n = 21.0 kg mol^{-1}, M_w = 35.3 kg mol^{-1}, PDI = 1.68. ^{1}H NMR (*o*-DCB-d$_4$, 400 MHz, 313 K, δ): 8.91 (s, 2H, Ar H), 8.36 (s, 2H, Ar H), 1.94-1.68 (bm, 8H, CH$_2$), 1.63-1.50 (bm, 8H, CH$_2$), 1.49-1.25 (bm, 40H, CH$_2$), 1.05 (t, *J* = 7 Hz, 12H, CH$_3$).

SiIDT-2FDTBT. Dark-blue solid (142 mg, 0.12 mmol, 55%). M_n = 26.4 kg mol^{-1}, M_w = 71.0 kg mol^{-1}, PDI = 2.69. ^{1}H NMR (*o*-DCB-d$_4$, 400 MHz, 313 K, δ): 8.52 (s, 2H, Ar H), 8.24-7.97 (m, 2H, Ar H), 7.88-7.44 (bm, 4H, Ar H), 1.86-1.71 (bm, 8H, CH$_2$), 1.69-1.27 (bm, 48H, CH$_2$), 1.17-1,01 (m, 12H, CH$_3$).

Device Fabrication and Testing: Top-gate, bottom-contact organic field effect transistors (FETs) were fabricated on glass with pentafluorobenzenethiol (PFBT) treated Au electrodes, CYTOP (900 nm) dielectric and Al gate. Polymer films were spin cast from *o*-

dichlorobenzene (10 mg/mL) solutions at a speed of 2000 rpm and annealed at 180 °C for 10 minutes. The carrier mobility of the films was assessed by measuring transfer curves in saturation (V_{DS} = -60 V) using a Keithley 4200 semiconductor parameter analyzer. The saturation mobility was determined by fitting a linear relationship of the square root of the drain current to gate potential in the range of -40 to -60 V and averaged over 3 devices.

All organic photovoltaic devices have a conventional device architecture, ITO/PEDOT:PSS/Polymer: $PC_{71}BM$/Ca/Al. The precoated ITO glass substrates were cleaned with acetone and isopropyl alcohol under sonification, followed by drying and oxygen plasma treatment during 7 minutes. A 30 nm layer of PEDOT:PSS was spin-coated onto the plasma-treated ITO substrate and baked at 150°C for 20 minutes. An 80 nm active layer consisting of a 1:3 blend of polymer, respectively 1:3.5 for the **SiIDT-BT** polymer, and $PC_{70}BM$ dissolved in *o*-dichlorobenzene (ODCB) was spin-coated on the PEDOT:PSS layer and then Ca (30 nm)/Al (100 nm) cathode was finally deposited by thermal evaporation under high vacuum (10^{-6} mbar) through a shadow mask. The pixel size, defined by the spatial overlap of the ITO anode and Ca/Al cathode, was 0.045 cm^2. The device characteristics were obtained using a xenon lamp at AM1.5 solar illumination (Oriel Instruments). Short circuit currents under AM1.5G conditions were obtained from the spectral response and convolution with the solar spectrum, measured with a Keithley source meter. Spectral response was measured under operation conditions using bias light from a 532 nm solid state laser (Edmund Optics). Monochromatic light from a 100 W tungsten halogen lamp in combination with monochromator (Oriel, Cornerstone 130) was modulated with a mechanical chopper. The response was recorded as the voltage over a 50 Ω resistance, using a lock-in amplifier (Stanford research Systems SR830). A calibrated Si cell was used as reference. All the device measurements were carried out behind a quartz window in a nitrogen filled container.

Supporting Information

Supporting Information is available from the Wiley Online Library or from the author.

Acknowledgements

The authors would like to acknowledge Dr. Ester Buchaca Domingo for the DSC measurements and the Imperial College High Performance Computing Service for providing the computing facilities to perform the quantum-mechanical calculations. This work was in part carried out under the EPSRC Project EP/F056710/1, EC FP7 ONE-P 245 Project 212311 and DPI Grant 678, with support from the Centre for Plastic Electronics at Imperial College London and the National Research Fund of Luxembourg.

Received: ((will be filled in by the editorial staff))
Revised: ((will be filled in by the editorial staff))
Published online: ((will be filled in by the editorial staff))

[1] a) I. McCulloch, M. Heeney, M. L. Chabinyc, D. DeLongchamp, R. J. Kline, M. Cölle, W. Duffy, D. Fischer, D. Gundlach, B. Hamadani, R. Hamilton, L. Richter, A. Salleo, M. Shkunov, D. Sparrowe, S. Tierney, W. Zhang, *Advanced Materials* **2009**, *21*, 1091; b) J. Sun, B. Zhang, H. E. Katz, *Advanced Functional Materials* **2011**, *21*, 29; c) Y. Liang, Z. Xu, J. Xia, S. Tsai, Y. Wu, G. Li, C. Ray, L. Yu, *Advanced Materials* **2010**, *22*, E135; d) A. Facchetti, *Chemistry of Materials* **2011**, *23*, 733.

[2] a) T. M. Clarke, A. M. Ballantyne, S. Tierney, M. Heeney, W. Duffy, I. McCulloch, J. Nelson, J. R. Durrant, *Journal of Physical Chemistry C* **2010**, *114*, 8068; b) C. J. Brabec, M. Heeney, I. McCulloch, J. Nelson, *Chemical Society Reviews* **2011**, *40*, 1185.

[3] a) G. Lu, H. Usta, C. Risko, L. Wang, A. Facchetti, M. A. Ratner, T. J. Marks, *Journal of the American Chemical Society* **2008**, *130*, 7670; b) W. Zhang, J. Smith, S. E. Watkins, R. Gysel, M. McGehee, A. Salleo, J. Kirkpatrick, S. Ashraf, T. Anthopoulos, M. Heeney, I. McCulloch, *Journal of the American Chemical Society* **2010**, *132*, 11437; c) Y.-C. Chen, C.-Y. Yu, Y.-L. Fan, L.-I. Hung, C.-P. Chen, C. Ting, *Chemical Communications* **2010**, *46*, 6503; d) Y. Zhang, J. Zou, H.-L. Yip, K.-S. Chen, D. F. Zeigler, Y. Sun, A. K.-Y. Jen, *Chemistry of Materials* **2011**, *23*, 2289.

[4] I. Osaka, R. D. McCullough, *Accounts of Chemical Research* **2008**, *41*, 1202.

[5] a) J. Wang, S. K. Hau, H. Yip, J. A. Davies, K. Chen, Y. Zhang, Y. Sun, A. K.-Y. Jen, *Chemistry of Materials* **2011**, *23*, 765; b) R. S. Ashraf, Z. Chen, D. Seok Leem, H. Bronstein, W. Zhang, B. Schroeder, Y. Geerts, J. Smith, S. Watkins, T. W. Anthopoulos, H. Sirringhaus, J. C. de Mello, M. Heeney, I. McCulloch, *Chemistry of Materials* **2011**, *23*, 768.

[6] J. Ohshita, M. Nodono, H. Kai, T. Watanabe, A. Kunai, K. Komaguchi, M. Shiotani, A. Adachi, K. Okita, Y. Harima, K. Yamashita, M. Ishikawa, *Organometallics* **1999**, *18*, 1453.

[7] a) S. C. Price, A. C. Stuart, L. Yang, H. Zhou, W. You, *Journal of the American Chemical Society* **2011**, *133*, 4625; b) H. Zhou, L. Yang, A. C. Stuart, S. C. Price, S. Liu, W. You, *Angewandte Chemie International Edition* **2011**, *50*, 2995.

[8] H. Chen, J. Hou, S. Zhang, Y. Liang, G. Yang, Y. Yang, L. Yu, Y. Wu, G. Li, *Nature Photonics* **2009**, *3*, 649.
[9] J. K. Park, J. Jo, J. Hwa Seo, J. Sun Moon, Y. Don Park, K. Lee, A. J. Heeger, G. C. Bazan, *Advanced Materials* **2011**, *23*, 2430.
[10] J. C. Slater, *Journal of Chemical Physics* **1964**, *41*, 3199.
[11] a) N. Hergué, P. Leriche, P. Blanchard, M. Allain, N. Gallego-Planas, P. Frère, J. Roncali, *New Journal of Chemistry* **2008**, *32*, 932; b) D.J. Crouch, P. J. Skabara, J. E. Lohr, J. J. W. McDouall, M. Heeney, I. McCulloch, D. Sparrowe, M. Shkunov, S. J. Coles, P. N. Horton, M. B. Hursthouse, *Chemistry of Materials* **2005**, *17*, 6567.
[12] C. Risko, M. D. McGehee, J-L. Brédas, *Chemical Science* **2011**, *2*, 1200.
[13] a) H. Bronstein, Z. Chen, R. S. Ashraf, W. Zhang, J. Du, J. R. Durrant, P. S. Tuladhar, K. Song, S. E. Watkins, Y. Geerts, M. M. Wienk, R. A. J. Janssen, T. Anthopoulos, H. Sirringhaus, M. Heeney, I. McCulloch, *Journal of the American Chemical Society* **2011**, *133*, 3272; b) X. Zhang, L. J. Richter, D. M. DeLongchamp, R. J. Kline, M. R. Hammond, I. McCulloch, M. Heeney, R. S. Ashraf, J. N. Smith, T. D. Anthopoulos, B. Schroeder, Y. H. Geerts, D. A. Fischer, M. F. Toney, *Journal of the American Chemical Society* **2011**, *133*, 15073; c) H. Bronstein, D. S. Leem, R. Hamilton, P. Woebkenberg, S. King, W. Zhang, R. S. Ashraf, M. Heeney, T. D. Anthopoulos, J. de Mello, I. McCulloch, *Macromolecules* **2011**, *44*, 6649.
[14] H. Jung Son, W. Wang, T. Xu, Y. Liang, Y. Wu, G. Li, L. Yu, *Journal of the American Chemical Society* **2011**, *133*.

Figures and captions:

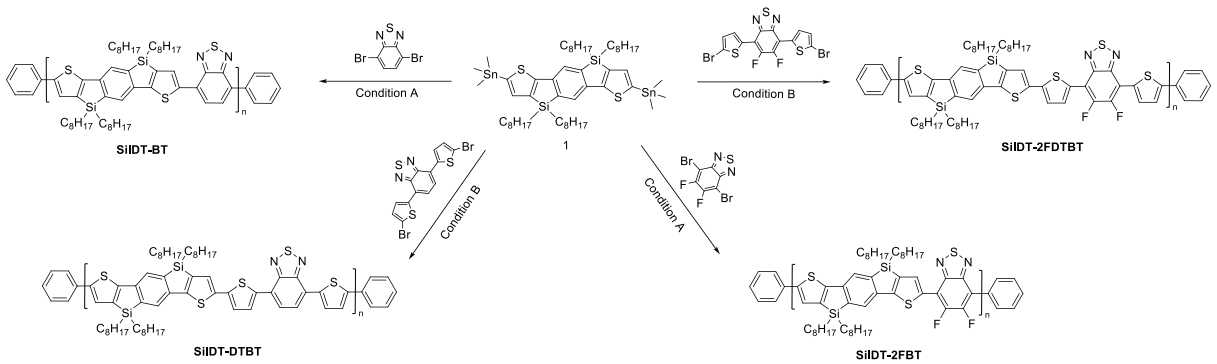

Scheme 1. Synthesis of the **SiIDT** based polymers; polymerization condition A: $Pd(PPh_3)_4$, *o*-xylene, microwave heating; polymerization condition B: $Pd_2(dba)_3$, $P(o\text{-}tol)_3$, chlorobenzene, microwave heating.

Table 1. Molecular weights and thermal properties of the polymers.

Polymer	M_n [kg/mol] [a]	M_w [kg/mol] [a]	PDI [a]	DP_n	T_d [°C] [b]
SiIDT-BT	30.0	58.9	1.96	34	443
SiIDT-DTBT	22.3	56.6	2.54	21	444
SiIDT-2FBT	21.0	35.3	1.68	23	428
SiIDT-2FDTBT	26.4	71.0	2.69	24	431

[a] Determined by GPC using polystyrene standards and chlorobenzene as eluent. [b] 5% weight loss temperatures measured by TGA under nitrogen atmosphere.

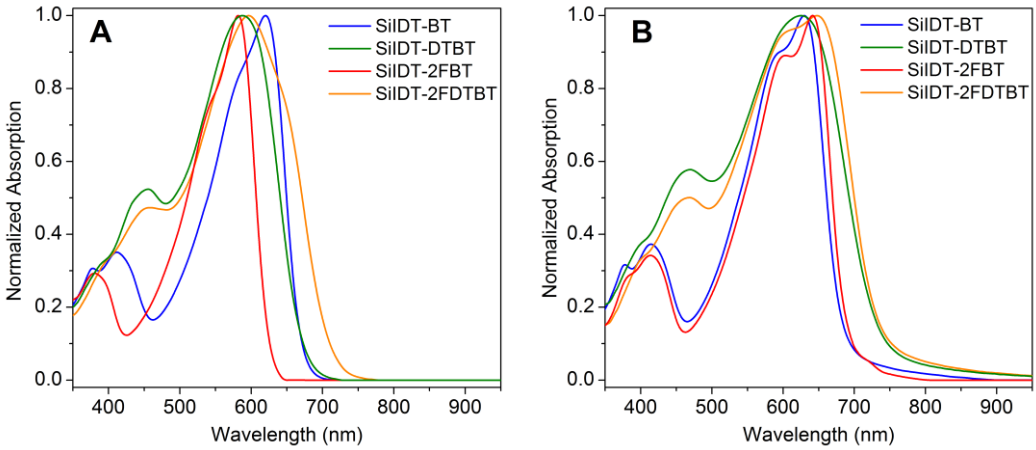

Figure 1. Normalized UV-*vis.* absorption spectra of **SiIDT** based polymers in dilute chlorobenzene solution (**A**) and thin-film (**B**), spin-cast from chlorobenzene.

Table 2. Optical properties and experimental and calculated energy levels of **SiIDT** based polymers.

			PESA	Cyclic voltammetry	DFT			
Polymer	λ_{max} soln. [nm] [a]	λ_{max} film [nm] [b]	HOMO / LUMO [eV] [c]	HOMO / LUMO [eV]	HOMO / LUMO [eV]	E_g^{opt} [eV]	E_g^{EC} [eV]	E_g^{calc} [eV]
SiIDT-BT	412, 620	414, 634	-5.4 / -3.6	-5.3 / -3.1	-4.7 / -3.0	1.8	2.2	1.7
SiIDT-DTBT	454, 588	468, 625	-5.0 / -3.3	-5.2 / -3.4	-4.6 / -3.0	1.7	1.8	1.6
SiIDT-2FBT	381, 582	413, 642	-5.4 / -3.6	-5.3 / -3.1	-4.8 / -3.1	1.8	2.2	1.7
SiIDT-2FDTBT	457, 597	468, 648	-5.1 / -3.4	-5.2 / -3.2	-4.7 / -3.1	1.7	2.0	1.6

[a] Measured in dilute chlorobenzene solution. [b] Spin-coated from 5 mg/mL chlorobenzene solution. [c] The LUMO energy is estimated by adding the absorption onset to the HOMO.

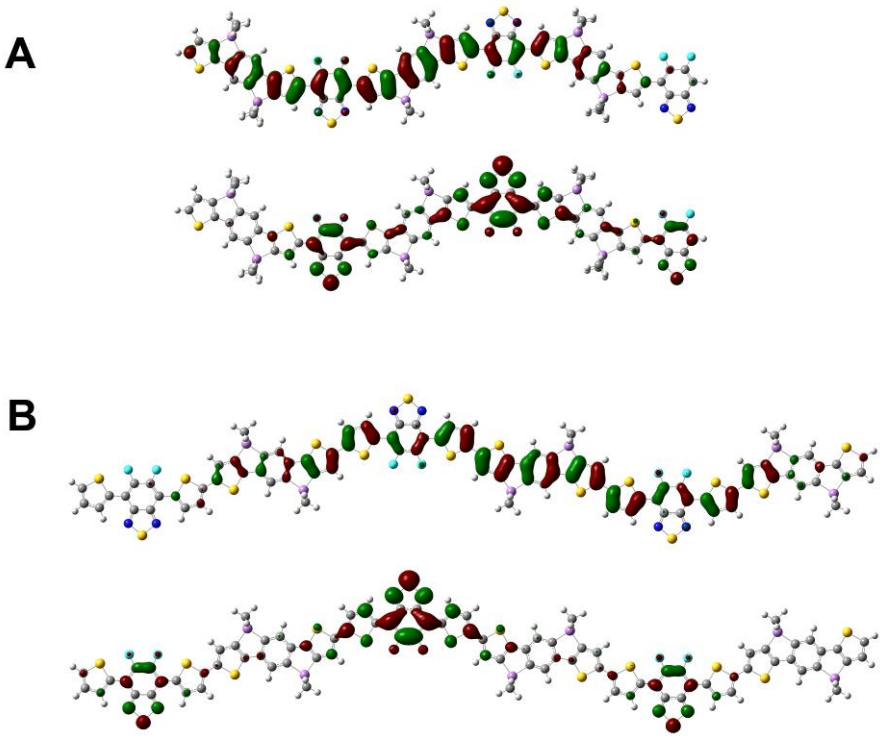

Figure 2. Energy-minimized structure (B3LYP/6-31G*) of a methyl-substituted **SiIDT-2FBT** (A) & **SiIDT-2FDTBT** (B) trimer with a visualisation of the HOMO (top) and LUMO (bottom) energy distributions.

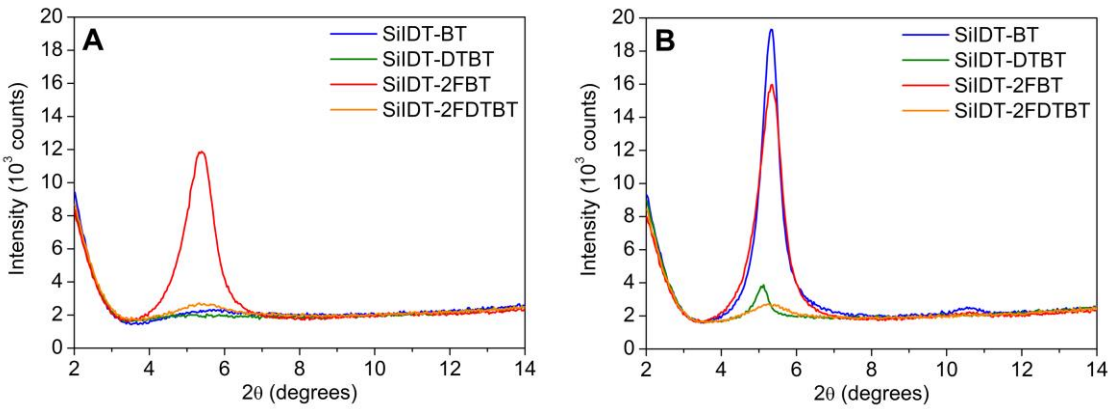

Figure 3. X-ray diffraction (XRD) patterns of drop-cast films of pristine **SiIDT** polymers on glass substrates (A) and after annealing at 180°C for 10 minutes under nitrogen atmosphere (B).

Table 3. OFET Device Characteristics of **SiIDT** polymers.

Polymer	μ_{sat} [cm²/Vs] [a]	μ_{lin} [cm²/Vs] [b]	I_{on}/I_{off} [a]
SiIDT-BT	0.014	0.011	~10^4
SiIDT-DTBT	0.28	0.25	~10^3
SiIDT-2FBT	0.004	0.002	~10^3
SiIDT-2FDTBT	0.19	0.10	~10^4

[a] μ_{sat} refer to the highest effective hole mobilities measured in the saturation regime. [b] μ_{lin} refer to the highest effective hole mobilities measured in the linear regime. The on-to-off ratios (I_{on}/I_{off}) were extracted from the linear regime.

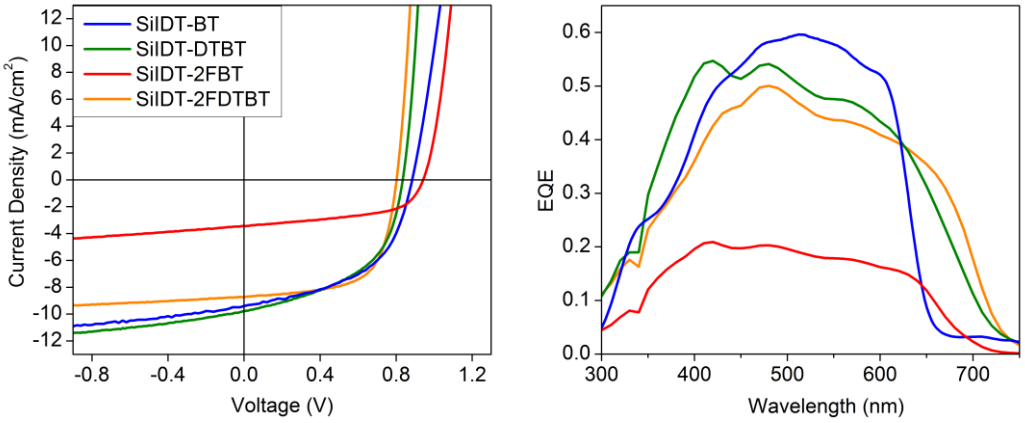

Figure 4. (left) J-V characteristics of **SiIDT** polymer:$PC_{71}BM$ solar cell under AM1.5 solar illumination and (right) external quantum efficiencies of the cells.

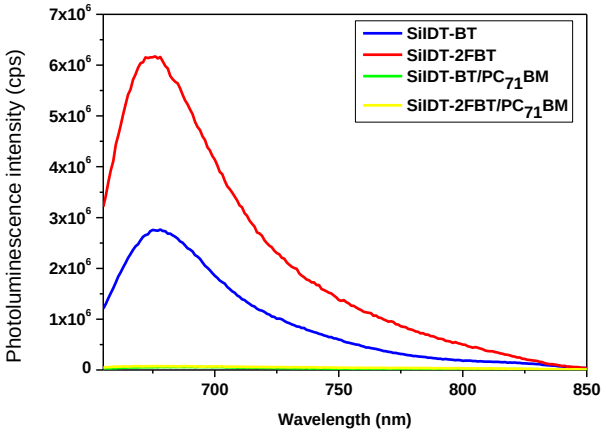

Figure 5. Photoluminescence spectra of thin films of **SiIDT-BT**, **SiIDT-2FBT**, **SiIDT-BT**/$PC_{71}BM$ and SiIDT-2FBT/$PC_{71}BM$. The samples were excited at 640 nm.

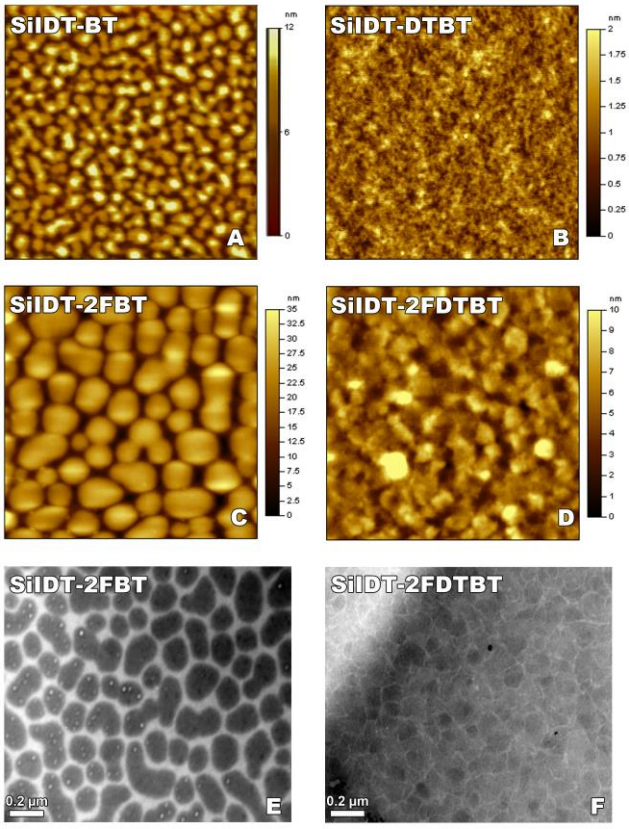

Figure 6. A to D: AFM topography images (2.0 µm x 2.0 µm) of 1:3w/w polymer/$PC_{71}BM$ blends (except for **SiIDT-BT** which is a 1:3.5 polymer:$PC_{71}BM$ blend). E and F: TEM images of **SiIDT-2FBT** and **SiIDT-2FDTBT.**

Table 4. OPV Device Characteristics of **SiIDT** polymers

Polymer	J_{SC} [mA/ cm^2]	V_{OC} [V]	FF	PCE [%]
SiIDT-BT	9.93	0.88	0.52	4.5
SiIDT-DTBT	8.75	0.83	0.50	3.6
SiIDT-2FBT	3.44	0.94	0.54	1.7
SiIDT-2FDTBT	8.36	0.80	0.64	4.3

Submitted to ADVANCED FUNCTIONAL MATERIALS

The table of contents entry.

Fluorine is introduced into silaindacenodithiophene based semi-conducting polymers with the aim to improve the photovoltaic as well as the charge carrier properties. The influence of the thienyl spacers and fluorine atoms on molecular packing and active layer morphology of the new polymers is investigated with regard to device performances.

Keywords: silaindacenodithiophene, hole mobility, solar cell, fluorine, conjugated polymers

Bob C. Schroeder, Zhenggang Huang, Raja Shahid Ashraf,* Jeremy Smith, Pasquale D' Angelo, Scott E. Watkins, Thomas D. Anthopoulos, James R. Durrant and Iain McCulloch

Silaindacenodithiophene based low band gap polymers – the effect of fluorine substitution on device performances and film morphologies.

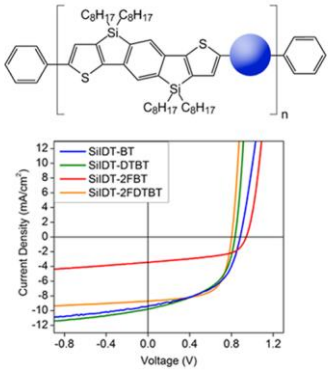

Supporting Information

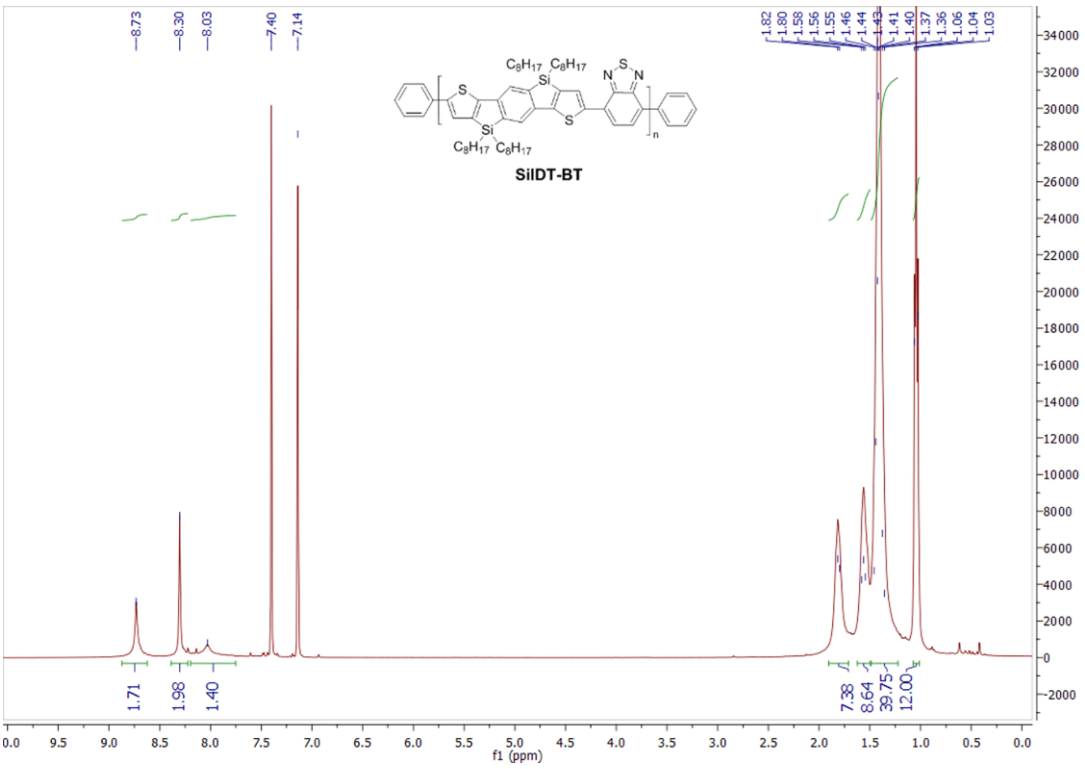

Figure S1. ^{1}H NMR spectrum of **SiIDT-BT** in d_4-1,2-dichlorobenzene at 313K.

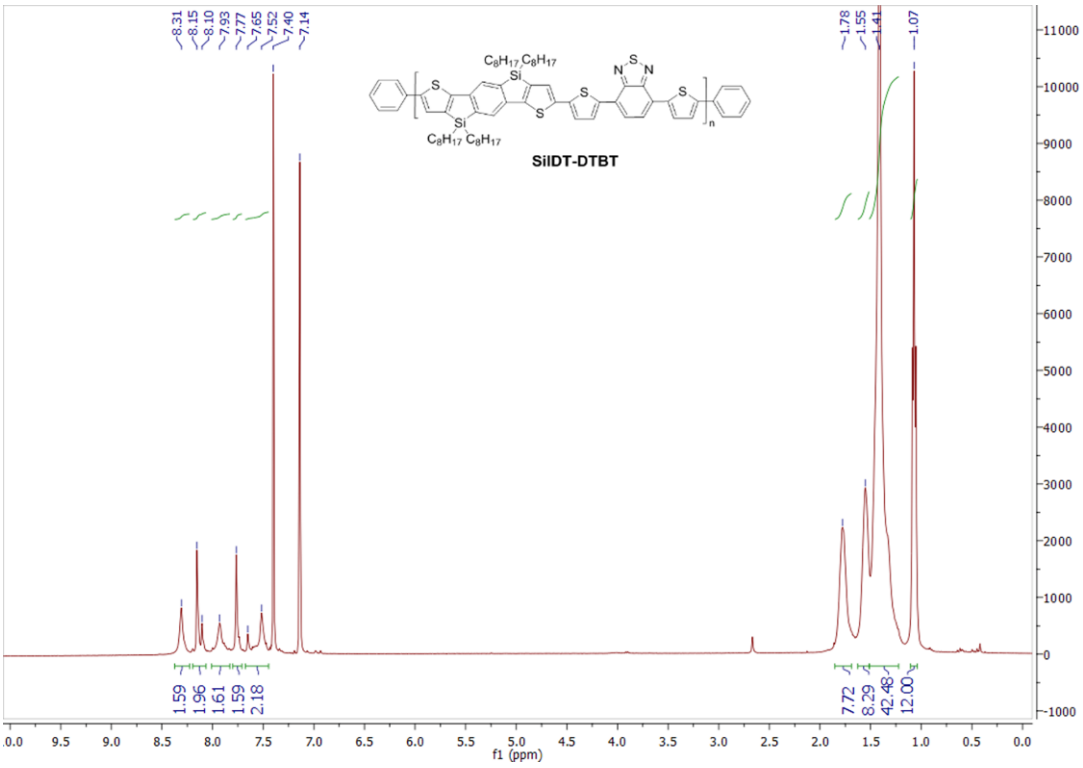

Figure S2. ^{1}H NMR spectrum of **SiIDT-DTBT** in d_4-1,2-dichlorobenzene at 313K.

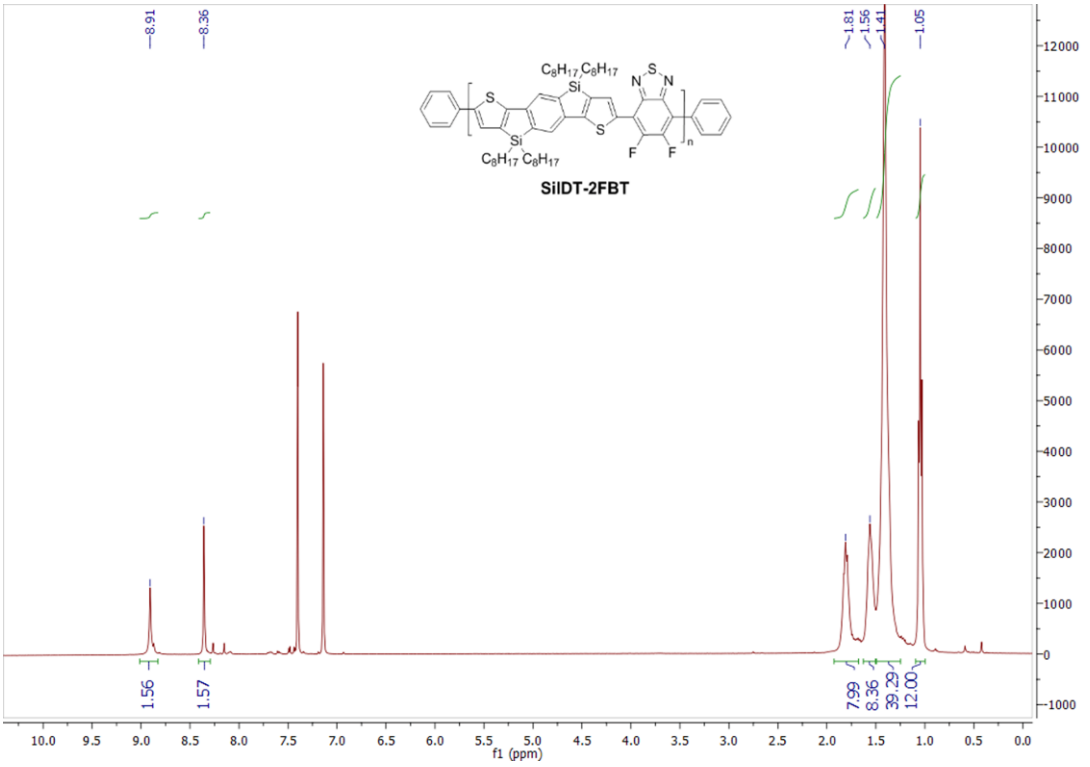

Figure S3. ^{1}H NMR spectrum of **SiIDT-2FBT** in d_4-1,2-dichlorobenzene at 313K.

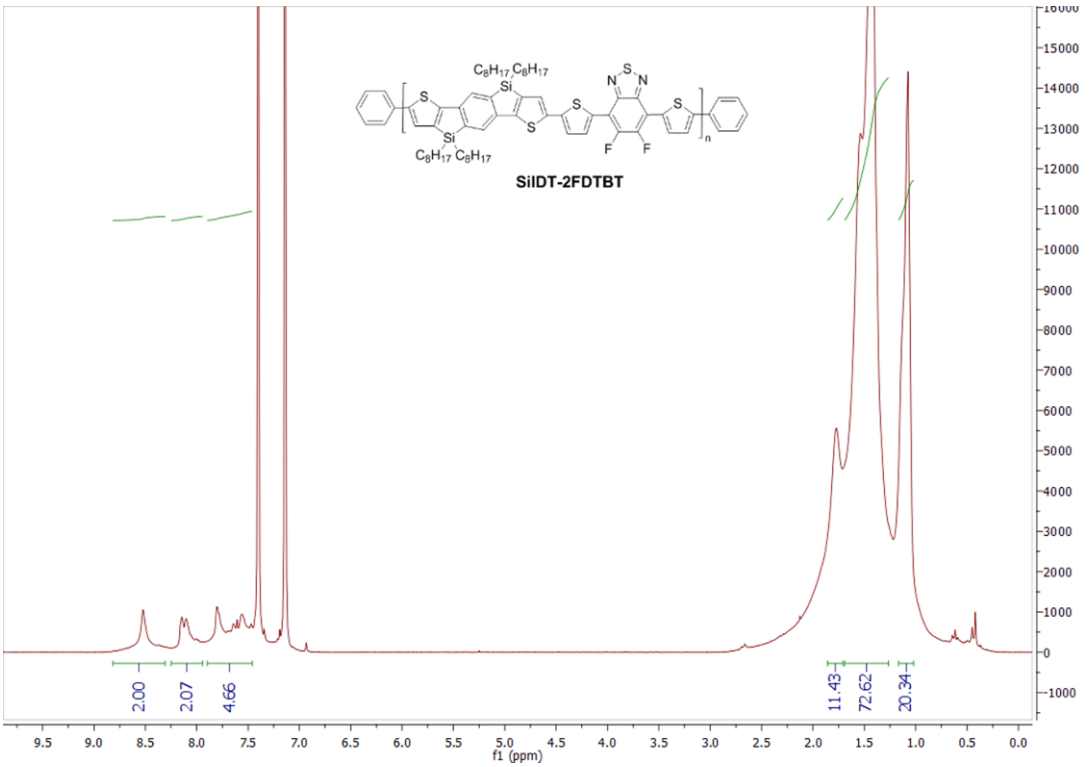

Figure S4. ^{1}H NMR spectrum of **SiIDT-2FDTBT** in d_4-1,2-dichlorobenzene at 313K.

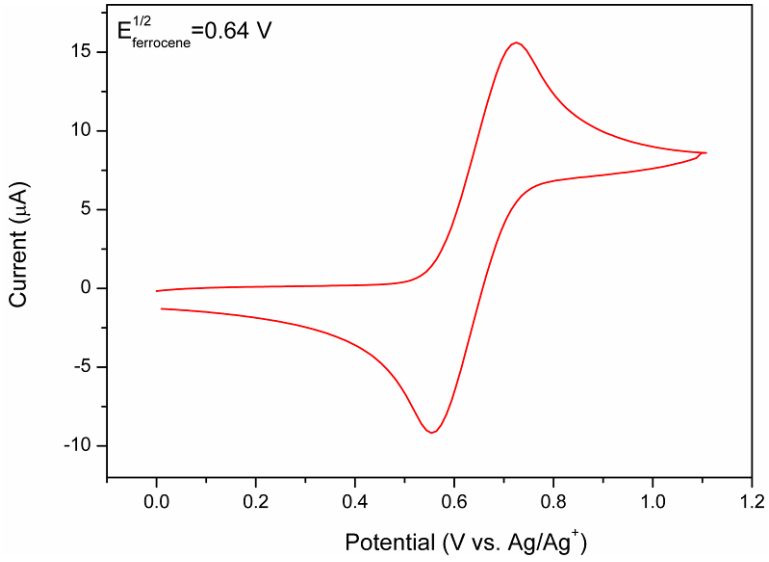

Figure S5. Cyclic Voltammetry curves of ferrocene in 0.1 M *n*-Bu_4NPF_6/CH_3CN at 25°C.

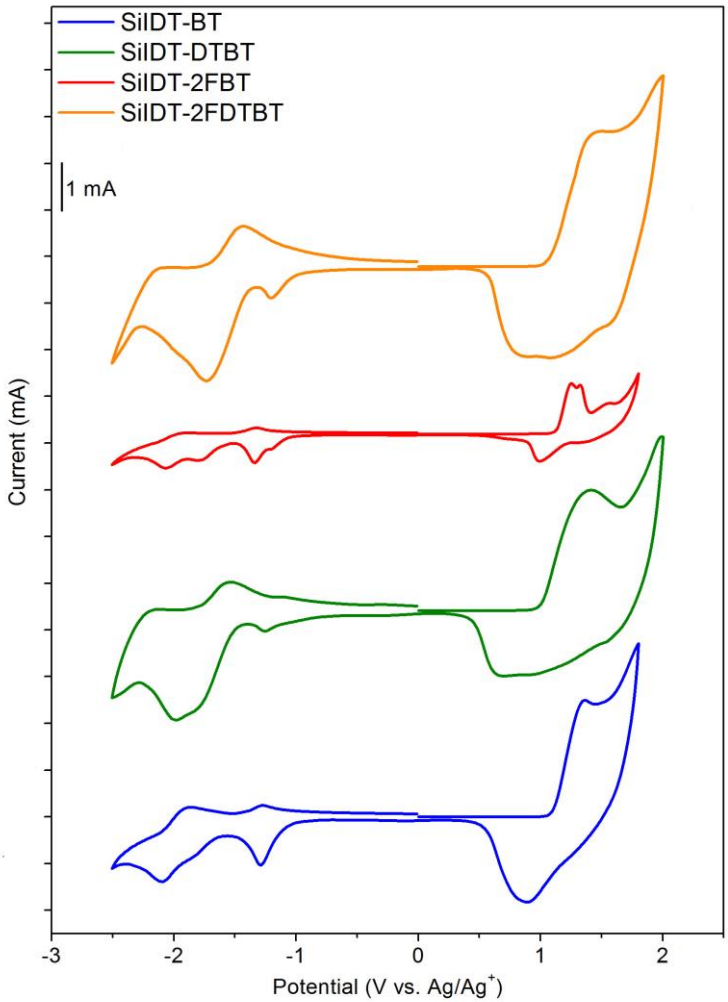

Figure S6. Cyclic Voltammetry curves of **SiIDT** polymer in 0.1 M *n*-Bu_4NPF_6/CH_3CN at 25°C.

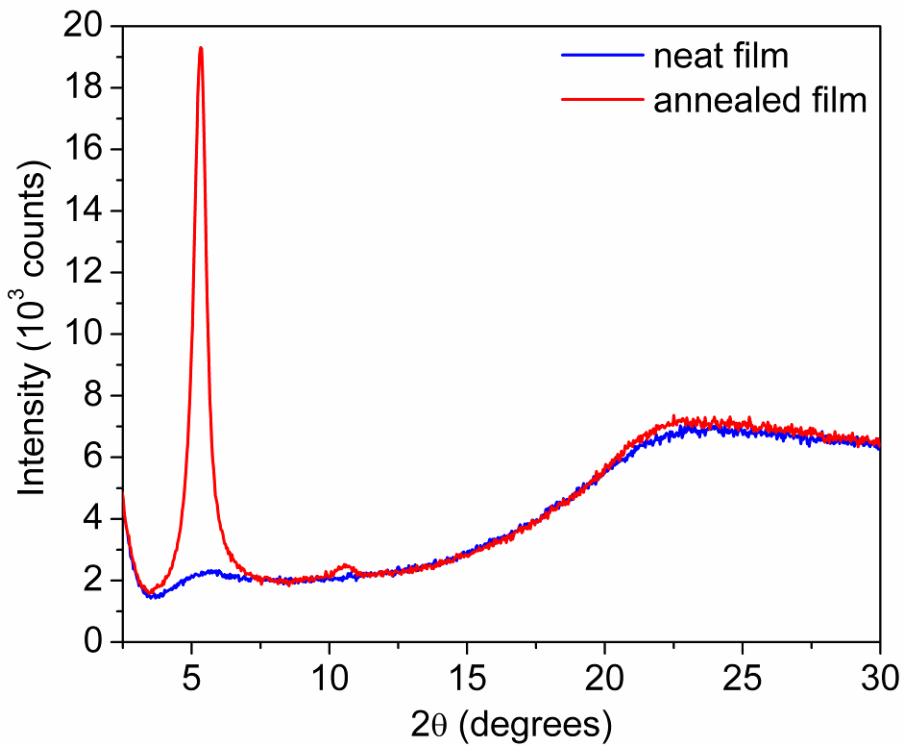

Figure S7. X-ray diffraction patterns of a drop-cast film of **SiIDT-BT** on glass substrates annealed at 180°C for 10 minutes under nitrogen atmosphere.

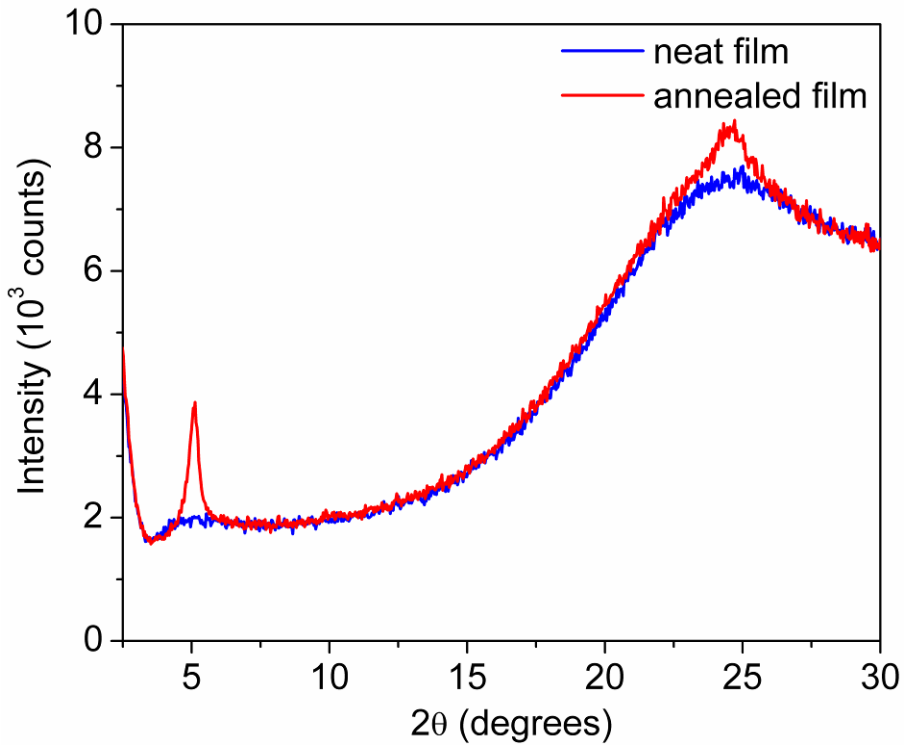

Figure S8. X-ray diffraction patterns of a drop-cast film of **SiIDT-DTBT** on glass substrates annealed at 180°C for 10 minutes under nitrogen atmosphere.

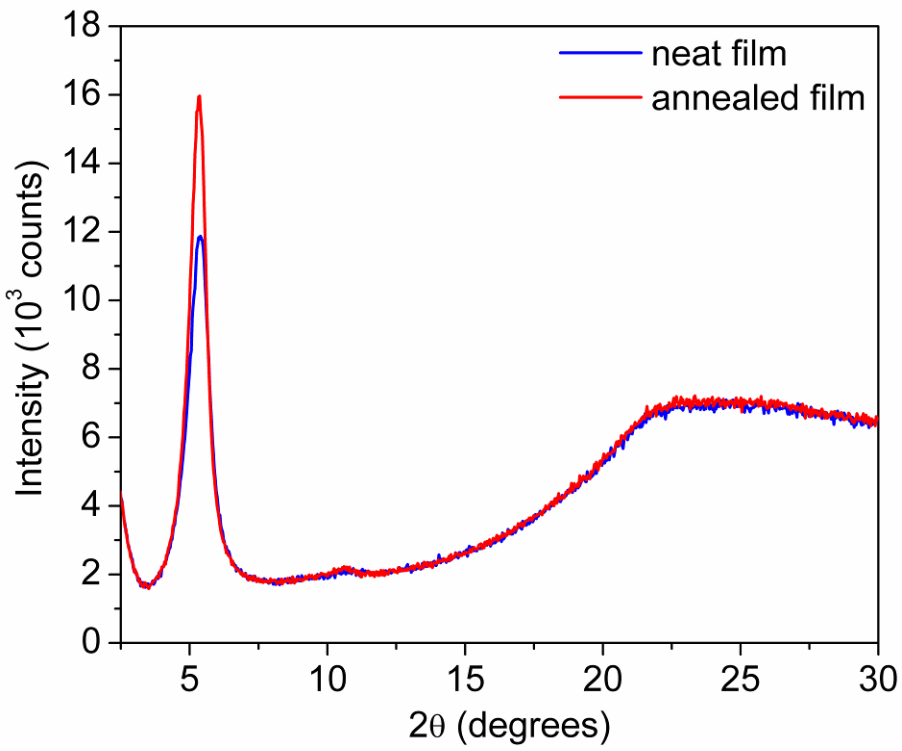

Figure S9. X-ray diffraction patterns of a drop-cast film of **SiIDT-2FBT** on glass substrates annealed at 180°C for 10 minutes under nitrogen atmosphere.

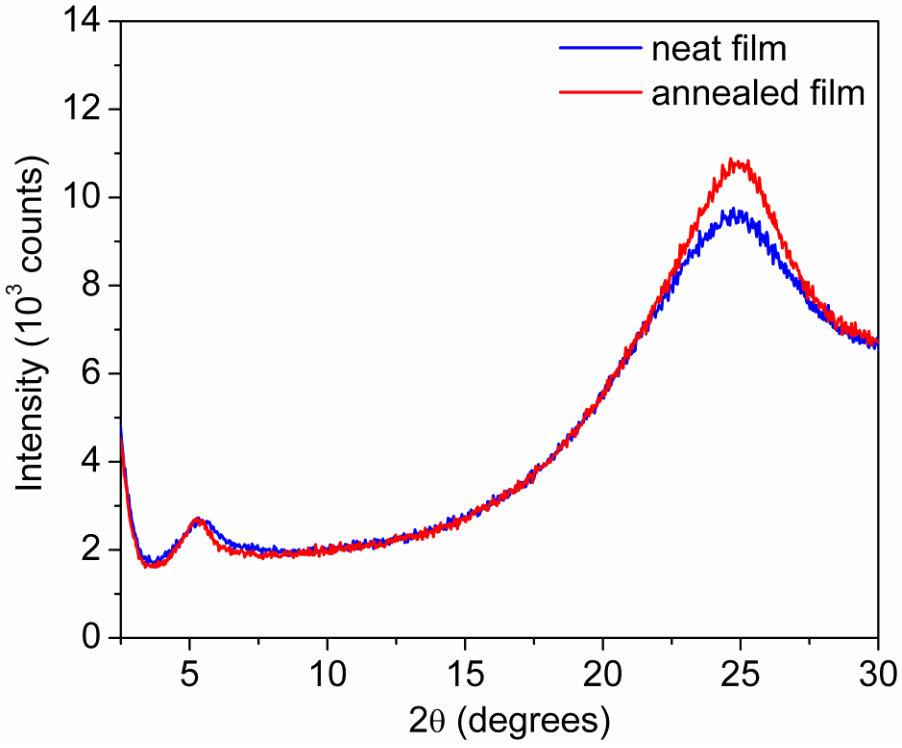

Figure S10. X-ray diffraction patterns of a drop-cast film of **SiIDT-2FDTBT** on glass substrates annealed at 180°C for 10 minutes under nitrogen atmosphere.

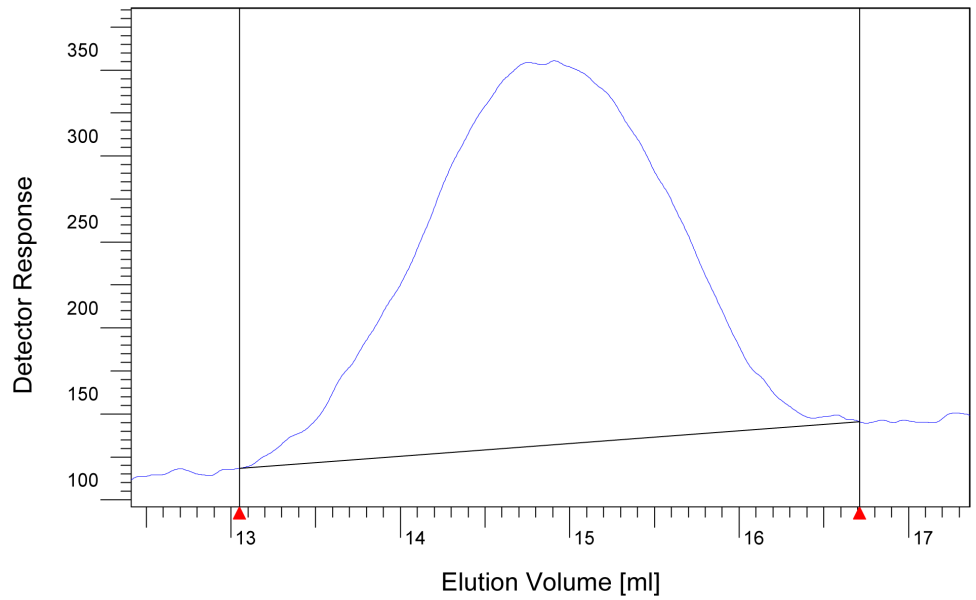

Figure S11. GPC trace of **SiIDT-BT**, M_n = 30.0 kg/mol, M_w = 58.9 kg/mol, PDI = 1.96.

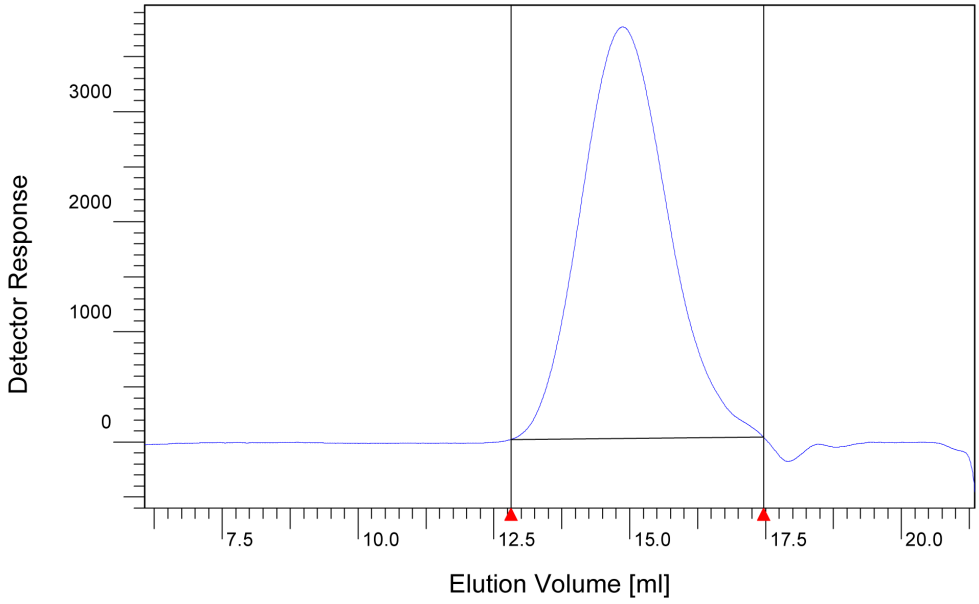

Figure S12. GPC trace of **SiIDT-DTBT**, M_n = 22.3 kg/mol, M_w = 56.6 kg/mol, PDI = 2.54.

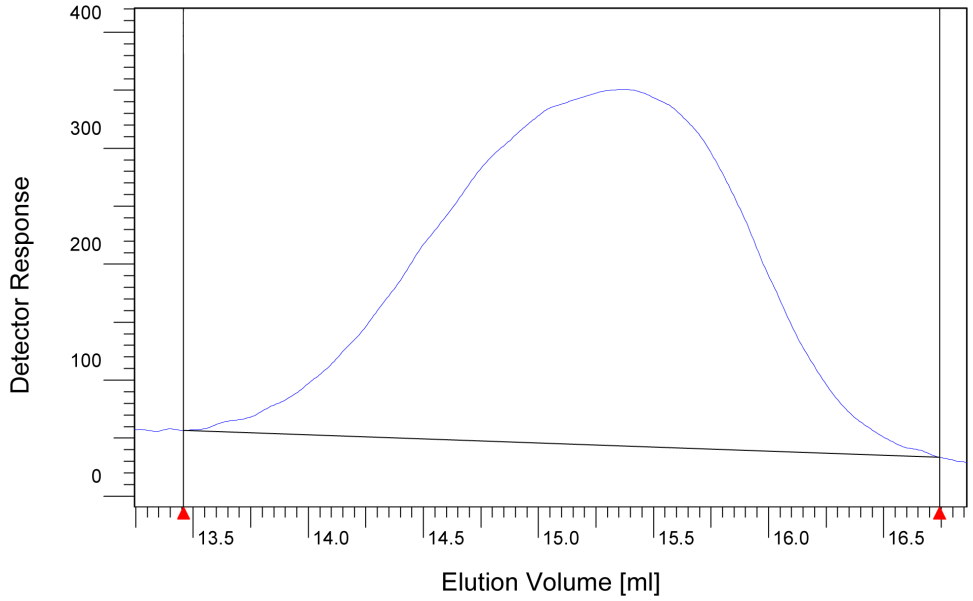

Figure S13. GPC trace of **SiIDT-2FBT**, M_n = 21.0 kg/mol, M_w = 35.3 kg/mol, PDI = 1.68.

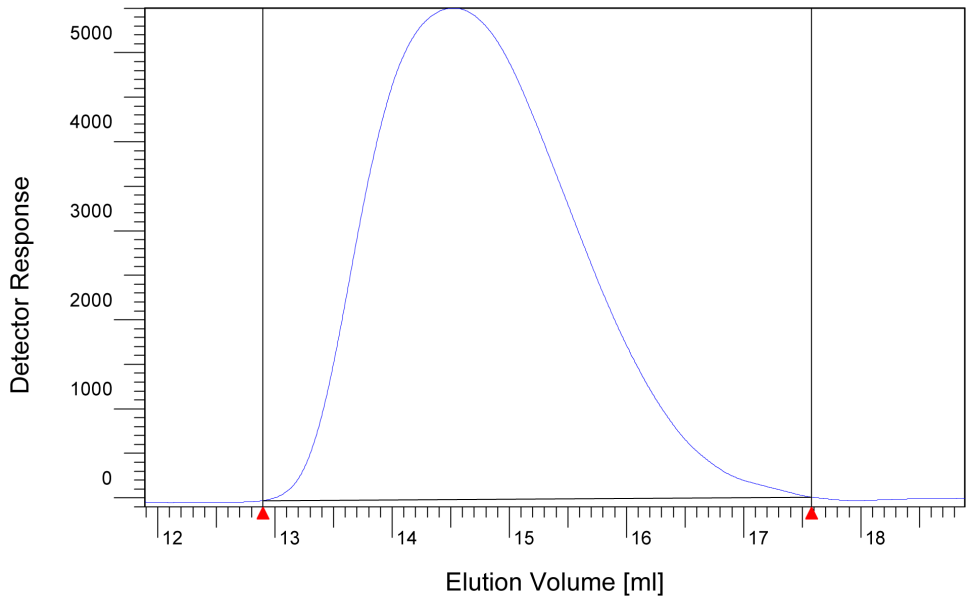

Figure S14. GPC trace of **SiIDT-2FDTBT**, M_n = 26.4 kg/mol, M_w = 71.0 kg/mol, PDI = 2.69.

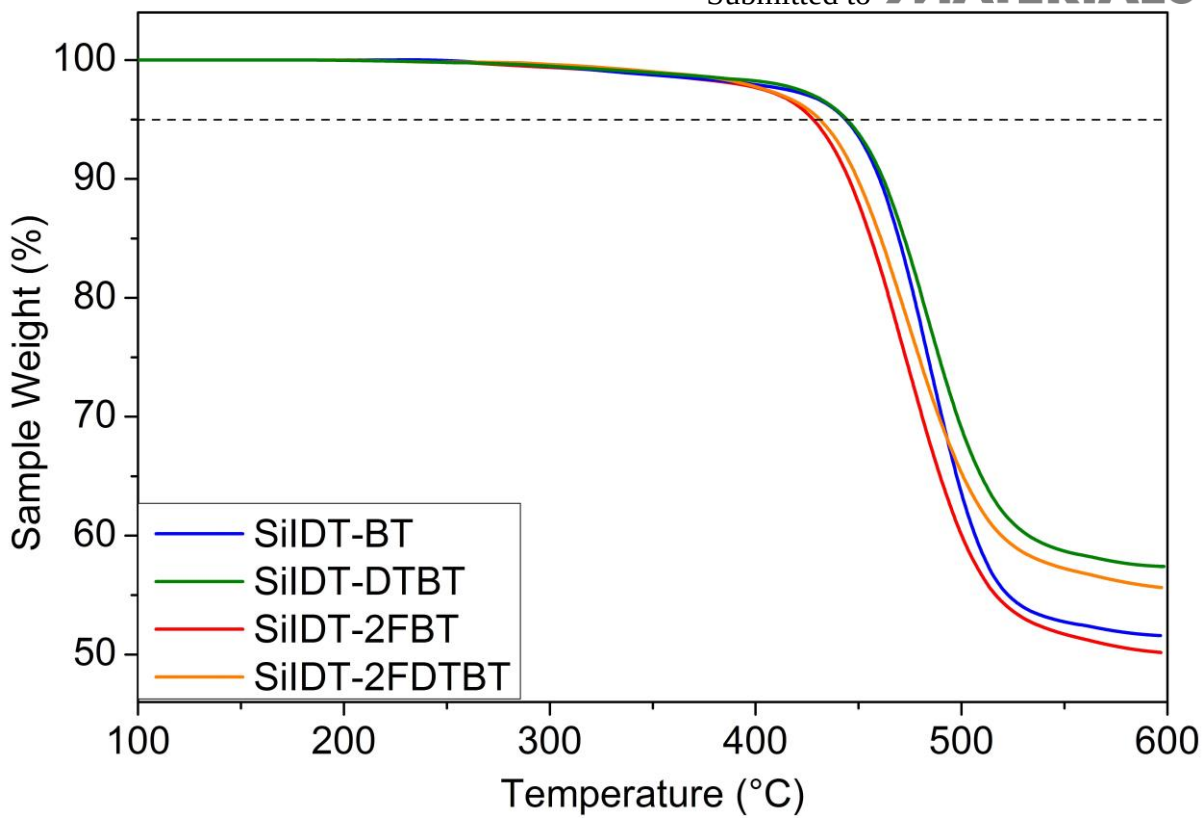

Figure S15. TGA thermograms of the **SiIDT** polymers with a heating rate of 10°C·min^{-1}.

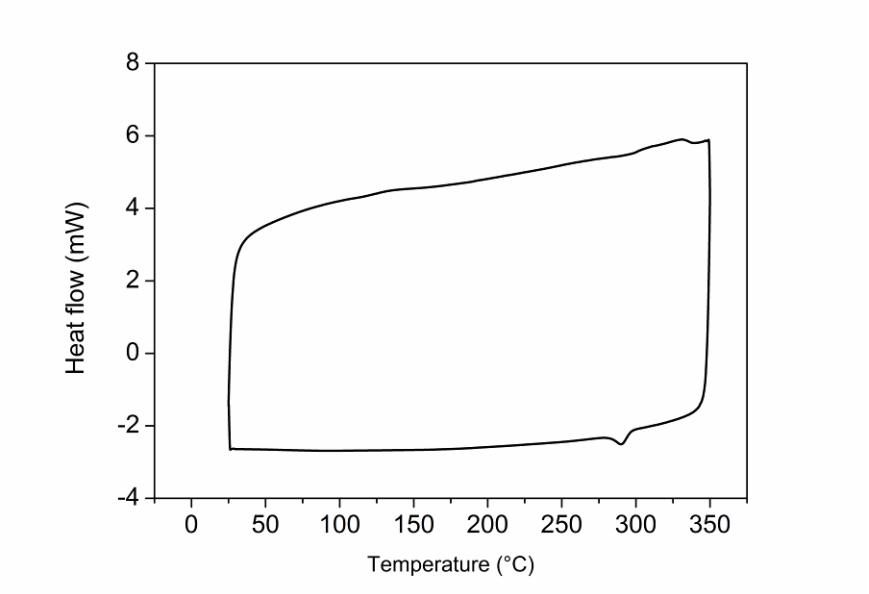

Figure S16. DSC trace of **SiIDT-BT**.

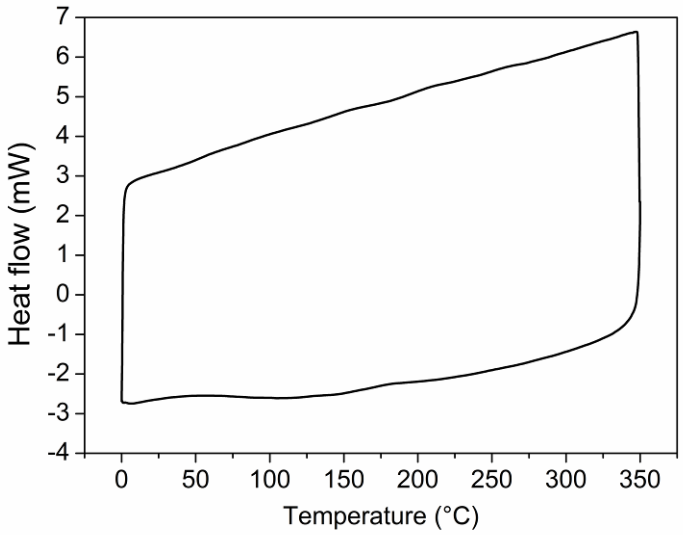

Figure S17. DSC trace of **SiIDT-DTBT**.

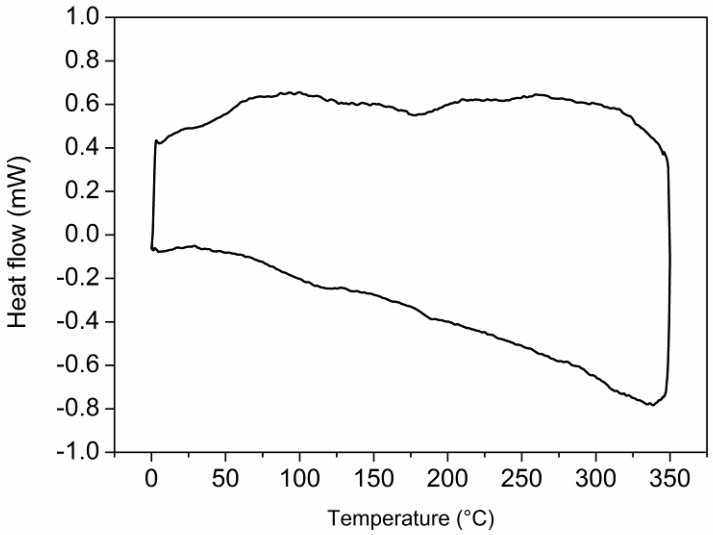

Figure S18. DSC trace of **SiIDT-2FBT**.

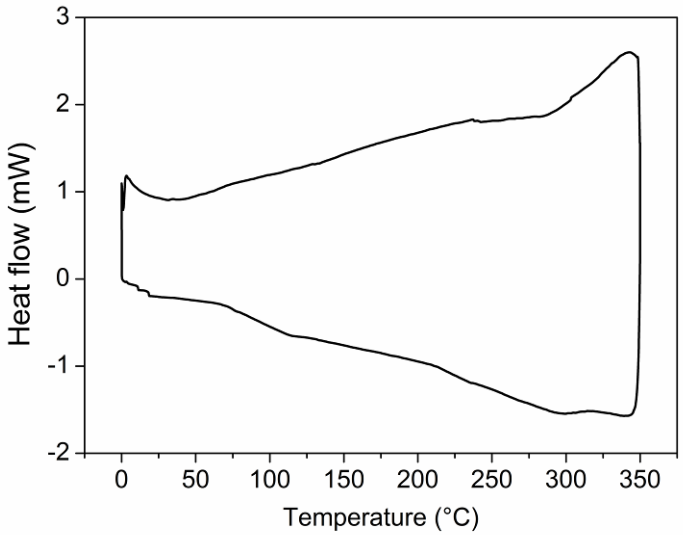

Figure S19. DSC trace of **SiIDT-2FDTBT**.

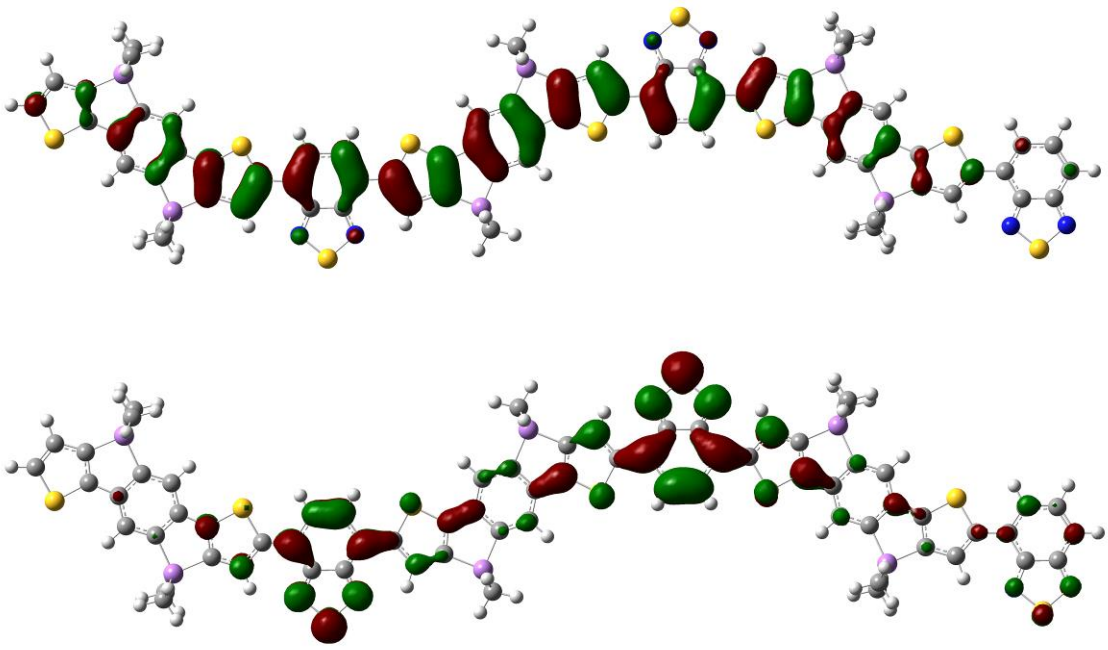

Figure S20. Energy-minimized structure (B3LYP/6-31G*) of a methyl-substituted **SiIDT-BT** trimer with a visualisation of the HOMO (top) and LUMO (bottom) energy distributions.

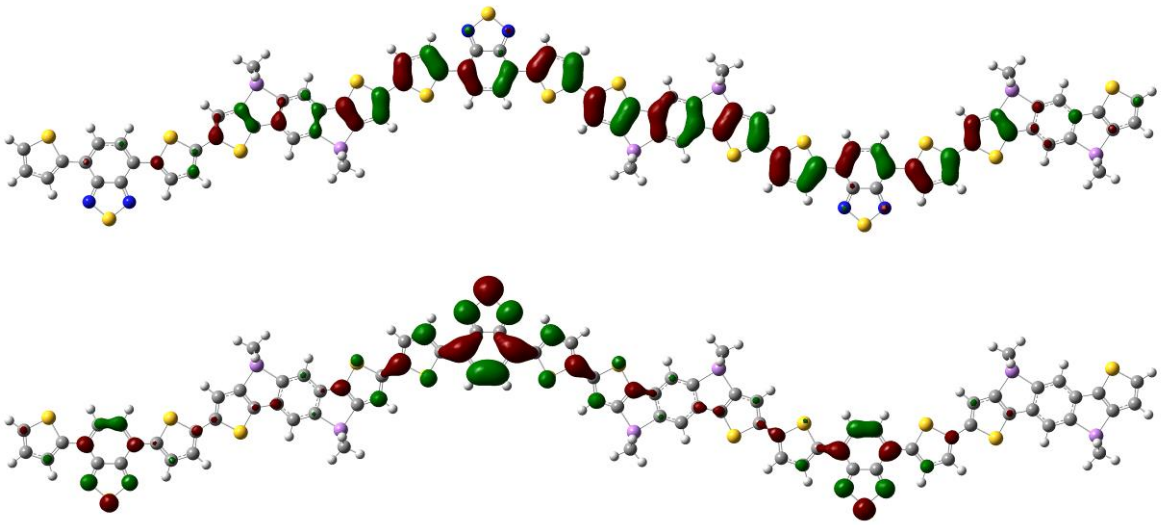

Figure S21. Energy-minimized structure (B3LYP/6-31G*) of a methyl-substituted **SiIDT-DTBT** trimer with a visualisation of the HOMO (top) and LUMO (bottom) energy distributions.

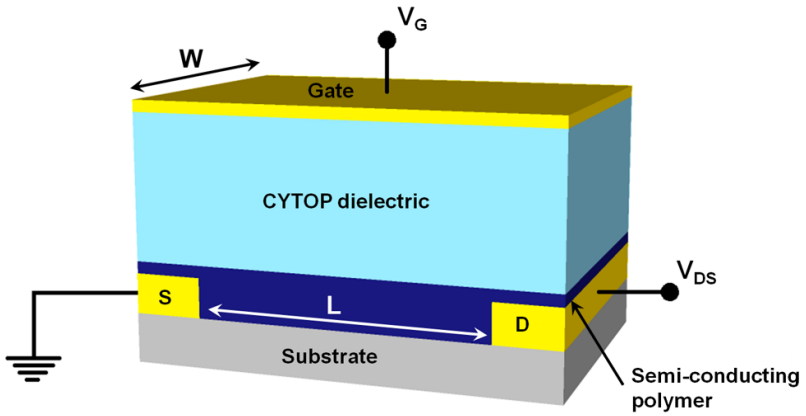

Figure S22. OFET device architecture.

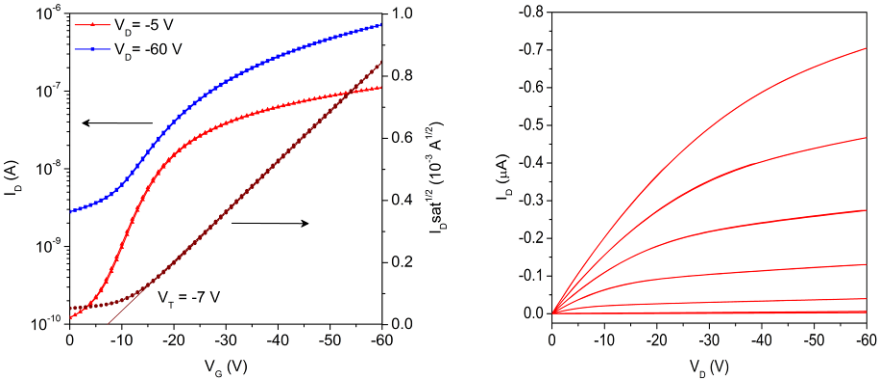

Figure S23. Transfer (left) and output (right) characteristics of a **SiIDT-BT** FET device spin-coated from *o*-dichlorobenzene (5 mg/mL) and annealed at 100°C for 5 min (L = 50 μm, W = 1.0 mm).

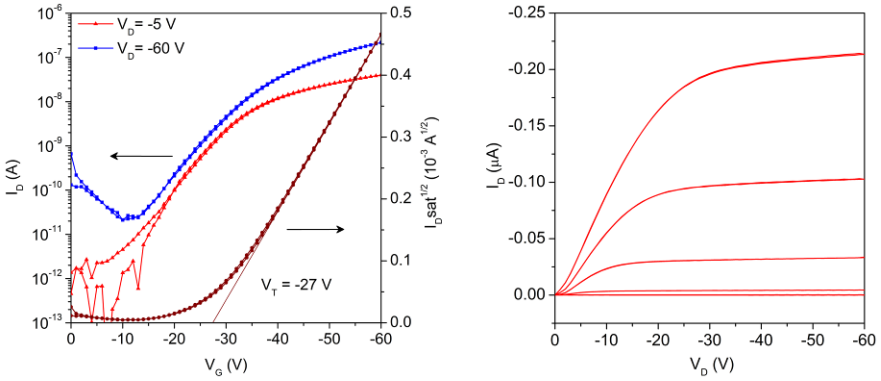

Figure S24. Transfer (left) and output (right) characteristics of a **SiIDT-BT** FET device spin-coated from *o*-dichlorobenzene (5 mg/mL) and annealed at 180°C for 10 min (L = 70 μm, W = 1.0 mm).

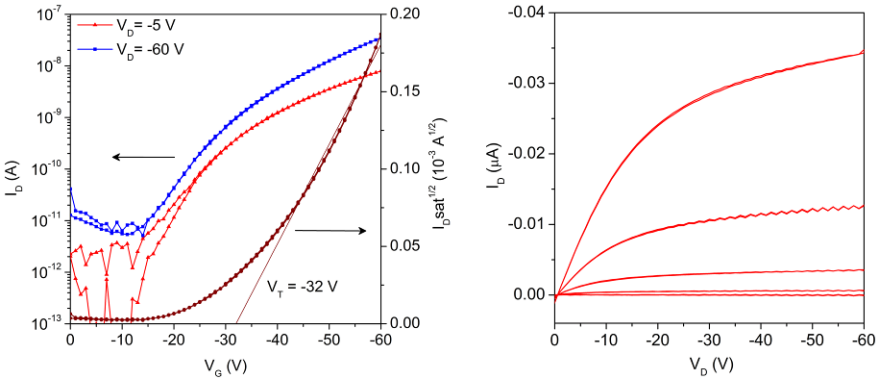

Figure S25. Transfer (left) and output (right) characteristics of a **SiIDT-2FBT** FET device spin-coated from *o*-dichlorobenzene (5 mg/mL) and annealed at 180°C for 10 min (L = 50 μm, W = 1.0 mm).

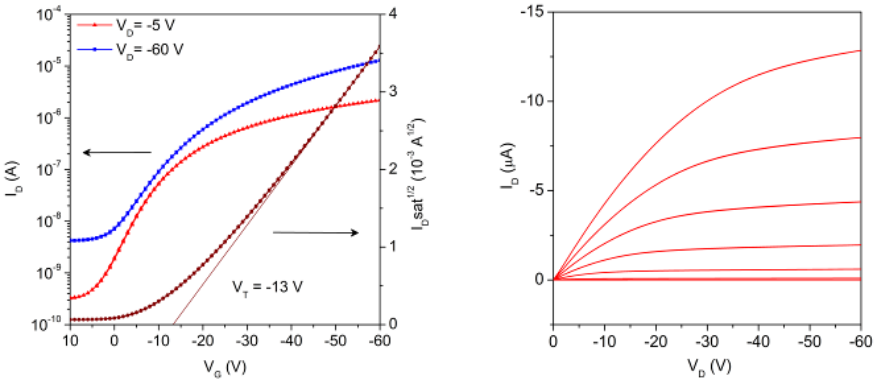

Figure S26. Transfer (left) and output (right) characteristics of a **SiIDT-DTBT** FET device spin-coated from *o*-dichlorobenzene (5 mg/mL) and annealed at 180°C for 10 min (L = 50 μm, W = 1.0 mm).

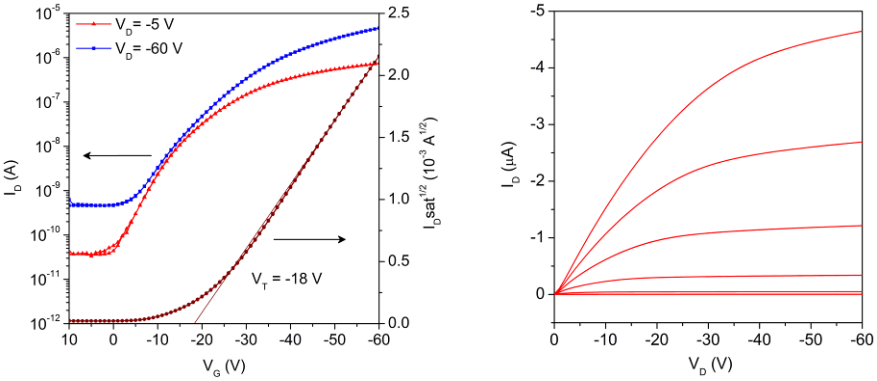

Figure S27. Transfer (left) and output (right) characteristics of a **SiIDT-2FDTBT** FET device spin-coated from *o*-dichlorobenzene (5 mg/mL) and annealed at 180°C for 10 min (L = 50 μm, W = 1.0 mm).

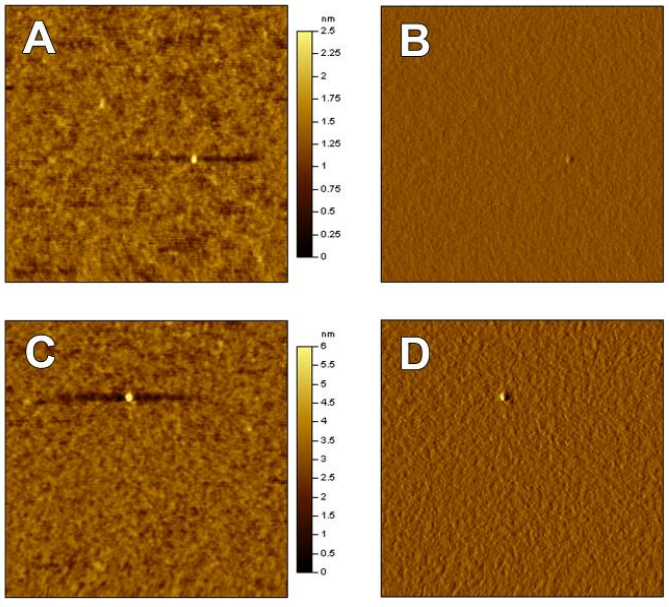

Figure S28. AFM topography (left column) and amplitude (right column) images (2.0 μm x 2.0 μm) of **SiIDT-BT** spin coated from 5 mg/mL *o*-dichlorobenzene solution on silicon substrate; neat film (A & B) and annealed film (C & D).